Sir2 tempers an intrinsic imbalance in origin licensing efficiency between early and late replicating euchromatin

Timothy Hoggard[1], Carolin A. Müller[2], Conrad A. Nieduszynski[2], Michael Weinreich[3], and Catherine A. Fox[1]

[1] Department of Biomolecular Chemistry, School of Medicine and Public Health, University of Wisconsin, Madison, WI 53706
[2]Sir William Dunn School of Pathology, University of Oxford, South Parks Road, Oxford, OX1 3RE, UK
[3]National Science Foundation, Division of Molecular and Cellular Biosciences, Alexandria, VA 22314

Abstract

The duplication and stability of a eukaryotic chromosome requires the function of multiple spatially distributed DNA replication origins. The chromosomal positions of MCM complexes determine where origins can function. While the biochemistry of MCM complex assembly onto DNA, or origin licensing, is defined, it is unclear how the chromosomal distribution of MCM complexes is achieved. We have elucidated a role for the Sir2 histone deacetylase in establishing the normal distribution of MCM complexes over *Saccharomyces cerevisiae* chromosomes. In the absence of Sir2, MCM complexes accumulated within early replicating euchromatin, which enhanced origin activity within these regions at the expense of late replicating euchromatin; thus late replicating euchromatin remained unduplicated at the end of S phase. We conclude that Sir2-mediated attenuation of MCM complex assembly within regions of the genome most receptive to origin licensing is necessary for the normal spatial distribution of MCM complexes and efficient duplication of yeast chromosomes.

Introduction

In eukaryotes, an adequate distribution of DNA replication origins across chromosomes is important for maintaining genome stability over the course of multiple rounds of cell division. For example, in human cells, chromosomal regions that contain a paucity of origins are linked to common fragile sites and cancer-associated deletions (Debatisse et al., 2012; Letessier et al., 2011; Miotto et al., 2016). In yeast, an artificial chromosome whose replication relies on origins positioned at the end of one arm is prone to breakage and shortening during cell division, while a comparable YAC containing origins distributed along its length remains intact (van Brabant et al., 2001). Furthermore, origin distribution in yeast affects gene expression (Müller and Nieduszynski, 2017). Extensive biochemical progress has established that the ability of a chromosomal region to function as an origin depends on how efficiently it supports two cell-cycle restricted molecular events (Bell and Labib, 2016). First, in G1-phase, a complex of the ORC (**o**rigin **r**ecognition **c**omplex) and the Cdc6 protein bound to DNA directs the assembly of two MCM hexamers that form a stable, catalytically inactive MCM complex encircling double-stranded DNA. Thus, the first essential molecular event required for origin function is MCM complex assembly (or loading) onto DNA, a.k.a. origin licensing. Second, in S-phase, kinases and additional proteins act on the MCM complex to convert it into two active replicative helicases each of which is comprised of a MCM hexamer, one GINS complex and a single Cdc45 (CMG helicase). The conversion of an MCM complex into two oppositely-oriented CMG helicases causes the unwinding of

DNA that allows for the initiation of DNA synthesis (a.k.a. origin activation; origin function; origin firing). Thus, the second essential molecular event required for origin function is MCM complex activation. While these core biochemical steps are defined, the mechanisms that determine the distribution of MCM complexes across chromosomes are incompletely understood (Newman et al., 2013; Das et al., 2015).

The budding yeast *Saccharomyces cerevisiae* is a useful model for examining mechanisms that establish the spatial and temporal distribution of origins across chromosomes. The power of yeast for addressing these issues derives in large part from the sequence-specific DNA binding of ORC, a feature unique to budding yeast (Bell and Stillman, 1992). In addition, the short G1-phase and high gene-density of this model eukaryote means that loaded MCM complexes remain closely associated with their ORC-dependent loading sites prior to their S-phase activation (Gros et al., 2015). These *S. cerevisiae*-specific origin attributes combined with multiple genome-wide experiments have allowed precise mapping of the ˜400 predominantly used yeast chromosomal origins (Feng et al., 2006; Nieduszynski et al., 2006; Raghuraman et al., 2001; Siow et al., 2012; Wyrick et al., 2001; Eaton et al., 2010). In addition, a number of available yeast genome-scale data sets allow for analyses of origin-adjacent chromatin features and origin functional properties (e.g. origin activation time in S-phase, origin efficiency, ORC binding mechanisms) (Weiner et al., 2015; McGuffee et al., 2013; Siow et al., 2012; Yabuki et al., 2002; Hoggard et al., 2013; Knott et al., 2012; Muller et al., 2010). Yeast origins can thus be parsed by selected structural and functional criteria, and comparisons of the resulting large origin groups can reveal important phenomena relevant to genome-scale origin control that would be challenging to glean from classic single-origin approaches.

Genome-scale studies of replication timing during S-phase have established that approximately half of yeast origins, distributed over the central regions of yeast chromosomes, are activated during the first portion of S-phase (referred to as early- or mid-S origins (Pohl et al., 2012; Raghuraman et al., 2001). The remaining origins, located at or near the chromosomal ends, function near the end of S-phase (late origins). This temporal-spatial distribution of origin function results in a reproducible pattern of chromosome replication in a proliferating population of yeast cells (**Figure 1**). Recent studies have identified specific non-histone chromatin-associated proteins, which are physically enriched within the chromatin comprising the central regions of chromosomes, that directly interact with a limiting S-phase kinase, the DDK (**D**bf4-**d**ependent **k**inase) (Fang et al., 2017; Natsume et al., 2013). DDK phosphorylates the MCM complex, triggering its conversion into two active CMG helicases, and is thus a key S-phase MCM complex activation protein present in limiting amounts relative to the number of loaded MCM complexes (Mantiero et al., 2011; Tanaka et al., 2011). Thus, specific local chromatin-mediated mechanisms help establish the spatial-temporal distribution of chromosomal origins.

In contrast to the recent advances in understanding how the S-phase MCM activation step can be controlled by local chromatin features to promote origin distribution, considerably less is known about how chromatin might differentially impinge on the G1-phase MCM complex loading step (Fang et al., 2017; Natsume et al., 2013). In fact, the documented robust impact of chromatin-control of the S-phase MCM complex activation step on the temporal-spatial distribution of yeast origins is most simply understood by assuming that MCM-complexes are reasonably distributed across yeast chromosomes. This assumption is consistent with extant data, although there is some disagreement in the literature about how equitably MCMs are distributed among yeast origins that fire at different times during S-phase (Das et al., 2015; Hoggard et al., 2018; Wyrick et al., 2001; Xu et al., 2006). Nevertheless, because yeast origins use a specific sequence for the ORC binding event that directs MCM complex loading, and MCM complexes can be detected in a variety of genomic regions, including those regions that are packaged into repressive heterochromatin, there has been no obvious *a priori* reason to invoke a role for chromatin in promoting the observed distribution of MCM complexes across yeast chromosomes.

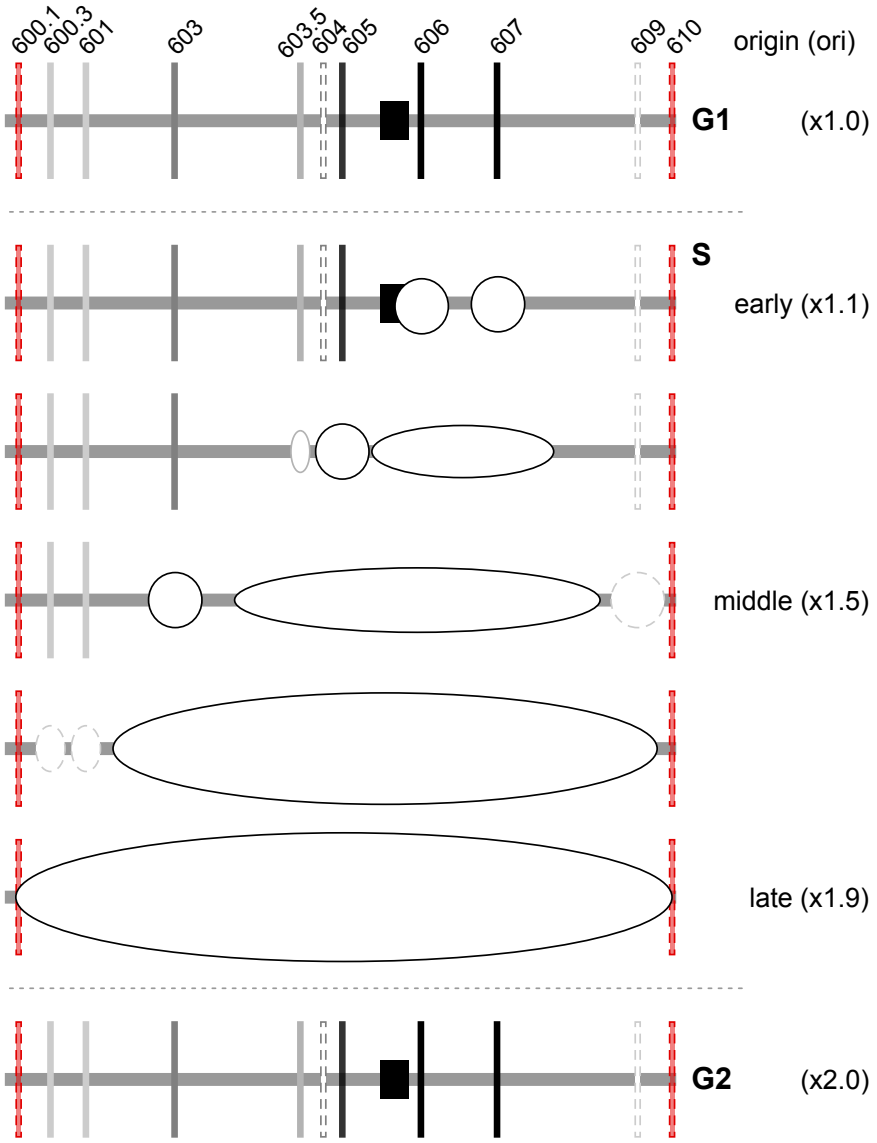

Figure 1: **The predominantly used origins of yeast chromosome VI.** The diagram depicts the average replication behavior of yeast chromosome VI (grey horizontal line) in a population of dividing yeast. The predominantly used origins that have been mapped and confirmed in multiple ensemble experiments are indicated with perpendicular lines. The square represents the centromere. Origins are activated during S phase. The origins with the highest probability of firing are depicted by black vertical lines. These origins are used in the majority of cell divisions and are activated in early S phase. Less efficient origins are depicted by gray or dotted vertical lines, with dotted lines indicating the least efficient of the confirmed origins mapped to this chromosome. An inefficient origin is used in only a fraction of cell cycles. The origins that exist within telomeres are inactive in most cell cycles and indicated by red vertical lines. Telomeres are packaged into Sir2-heterochromatin and their origins become active in *sir2Δ* cells.

In a recent study, our group reported that the yeast heterochromatin-associated histone deacetylase, Sir2, inhibited MCM complex loading by acting to deacetylate lysine 16 of histone H4 (H4K16) at origin-adjacent nucleosomes within euchromatin, providing the first evidence that a native chromatin structure at

yeast origins could inhibit origin licensing (Hoggard et al., 2018). Specifically, the nucleosomes immediately adjacent to euchromatic origins are depleted for H4K16ac, the known Sir2 substrate, and this depletion is *SIR2*-dependent. In addition, a second heterochromatin-associated protein, the nucleosome-binding protein Sir3, is detectable at these origin-adjacent nucleosomes. While the direct action of Sir2/3 at euchromatic origins was unanticipated given their paradigmatic roles as heterochromatic proteins, an earlier series of genetic suppression experiments provide evidence that these Sir2-chromatin features at euchromatic origins are indeed functional (Crampton et al., 2008; Pappas et al., 2004). Specifically, inactivating mutations in *SIR2* or *SIR3*, as well as mutations in histone genes predicted to phenocopy loss-of-function mutations in these *SIR* genes, robustly suppress the temperature-sensitive growth defect of *cdc6-4*, an allele of *CDC6* that fails to license yeast origins at the non-permissive growth temperature (Crampton et al., 2008; Hoggard et al., 2018). Indeed, in *sir2*Δ *cdc6-4* mutant yeast cells, MCM loading can be detected at most yeast origins, including the majority of euchromatic origins, even when cells are cultured at the non-permissive temperature for *cdc6-4* (Hoggard et al., 2018). Importantly, loss of *SIR2* function can suppress other temperature-sensitive alleles in genes encoding proteins required for MCM loading (Pappas et al., 2004). Thus, the levels and/or activities of the MCM complex loading proteins have evolved to function within a locally repressive chromatin environment established by direct Sir2 function. However, to date the effects of Sir2 on MCM complex loading have been documented in mutant cells that contain a genetically compromised MCM complex loading pathway. In addition, and in contrast to the proteins that function directly in origin licensing, Sir proteins are non-essential. Therefore, while prior work establishes that functionally relevant Sir2-chromatin forms at euchromatic origins with the potential to inhibit MCM complex loading, a physiological role for this chromatin effect in wild-type yeast has not been addressed.

In this study, quantitative analyses of several biologically independent genome-scale data sets mapping MCM binding (MCM ChIP-Seq) and replication timing (Sort-Seq) were performed to address the role of *SIR2* in origin licensing and replication in wild-type yeast. *SIR2* substantially attenuated MCM complex loading at telomeric X-origins, known to be packaged into Sir2-heterochromatin, providing the first evidence that Sir2-heterochromatin could inhibit origin function at the level of origin licensing. Considering Sir2 effects on euchromatin, and in contrast to initial expectations, efficient euchromatic origins that fire in early S-phase (early origins) were more sensitive to the negative impact of Sir2 than euchromatic origins that fire later in S-phase (late origins). Consistent with this observation, key molecular features of Sir2-chromatin were more abundant at early compared to late euchromatic origins. Sort-Seq and two-dimensional origin mapping experiments indicated that early euchromatic origins, despite their already high efficiency in wild-type cells, functioned with even greater efficiencies in *sir2*Δ cells, supporting the conclusion that these origins were competing more effectively for functional MCM complexes in the absence of Sir2. Finally, Sort-Seq data provided evidence that *SIR2* was required for completing the duplication of several late-replicating euchromatic regions by the end of S-phase via a mechanism that was independent of the replication capacity of the rDNA locus, which can act indirectly to confer *SIR2* control on yeast chromosome duplication (Foss et al., 2017; Yoshida et al., 2014). We conclude that Sir2-chromatin-mediated attenuation of origin licensing at individual origins prevented genomic regions with the greatest intrinsic potential for MCM complex loading from sequestering MCM complexes, thereby ensuring a more equitable distribution of licensed origins across chromosomes. The relatively equitable distribution of MCM complexes across yeast chromosomes was in turn important for completing duplication of the euchromatic genome (i.e. gene-coding regions) within S-phase. These findings are the first example of a chromatin-mediated mechanism that acts at individual origins to promote the normal genome-scale distribution of MCM complexes.

Results

Early origins were enriched among euchromatic origins most responsive to *SIR2*.

A negative role for *SIR2* in MCM complex loading is evident in haploid *cdc6-4* mutant yeast grown at non-permissive temperature (NPT, 37°C) (Crampton et al., 2008; Hoggard et al., 2018; Pappas et al.,

2004). Specifically, MCM ChIP-Seq signals (MCM signals) are lost at chromosomal origins in *cdc6-4* cells at 37°C, but restored at most origins, including many euchromatic origins, in *cdc6-4 sir2*Δ cells (Hoggard et al., 2018). However, not all euchromatic origins in *cdc6-4 sir2*Δ cells are rescued to the same degree. Sir2-heterochromatic regions are late replicating and inhibitory to origin function (Stevenson and Gottschling, 1999; Yoshida et al., 2014; Palacios DeBeer et al., 2003; Palacios DeBeer and Fox, 1999), therefore our initial expectation was that the euchromatic origins that were most effectively rescued for MCM association in *cdc6-4 sir2*Δ cells would be inefficient and/or late origins. However, we found that the euchromatic origins most responsive to *SIR2* (i.e. defined as origins that showed the greatest MCM signal rescue in *cdc6-4 sir2*Δ cells (Hoggard et al., 2018)) were enriched for early origins, and, conversely, that the euchromatic origins that showed the lowest Sir2-responsiveness were enriched for origins where a defined Trep value, an indicator of an origin's fragment's replication time in S-phase, could not be assigned (not-measured origins) (**Figure 2A**) (Yabuki et al., 2002). Further analyses revealed that 90% of the origins classified as not-measured in the replication timing experiment were so inefficient that they were not detected in a genome-wide origin efficiency study (McGuffee et al., 2013) (**S1 Figure**). Therefore, within euchromatin, Sir2 inhibited MCM complex loading more significantly at early origins compared to inefficient origins.

To further examine this counterintuitive outcome, we examined MCM signals at higher resolution using data generated from three independent biological experiments (**Figure 2B-D**). In these analyses, we determined the distribution of MCM signal (median ± 1 quartile) for each nucleotide spanning 501 bp origin-containing fragments, aligned with respect to the T-rich strand of their ORC binding sites for various groups of origins. Data were plotted for wild-type (*CDC6 SIR2*), *cdc6-4* (*cdc6-4 SIR2*) and *cdc6-4 sir2*Δ cells (**Figure 2B**). MCM signals, while abolished in *cdc6-4* cells, were rescued at euchromatic origins in *cdc6-4 sir2*Δ cells (**Figure 2C**). However, origin groups defined as having the highest *SIR2*-reponsiveness based on their initial lower-resolution assignments showed the greatest relative MCM signal rescue in *cdc6-4 sir2*Δ cells. These data were consistent with the lower resolution approach used to generate the data in **Figure 2A**, validating the analysis method. This approach was then applied to euchromatic origins parsed by their replication times (Trep), an origin attribute that was assigned in a completely independent study (Yabuki et al., 2002) (**Figure 2D**). Consistent with the lower-resolution analysis in **Figure 2A**, early origins and mid-S-phase origins (mid) were rescued to a greater extent in *cdc6-4 sir2*Δ cells relative to their counterparts in wild-type cells, while both late and not-measured origins were rescued to lesser extents. In these higher-resolution analyses, both the late and not-measured origin groups behaved similarly, showing relatively weak levels of rescue. Additional assessments using origins parsed by an efficiency metric or by Fkh1/2 regulation, a property causally linked to origin timing, produced similar trends (Knott et al., 2012; McGuffee et al., 2013)(**S2 Figure**). Thus, Sir2-control of euchromatic origins, as measured by the degree to which a *sir2*Δ mutation suppressed the MCM loading defect of a *cdc6-4* mutant, was more effective at early, efficient origins than at late or inefficient origins.

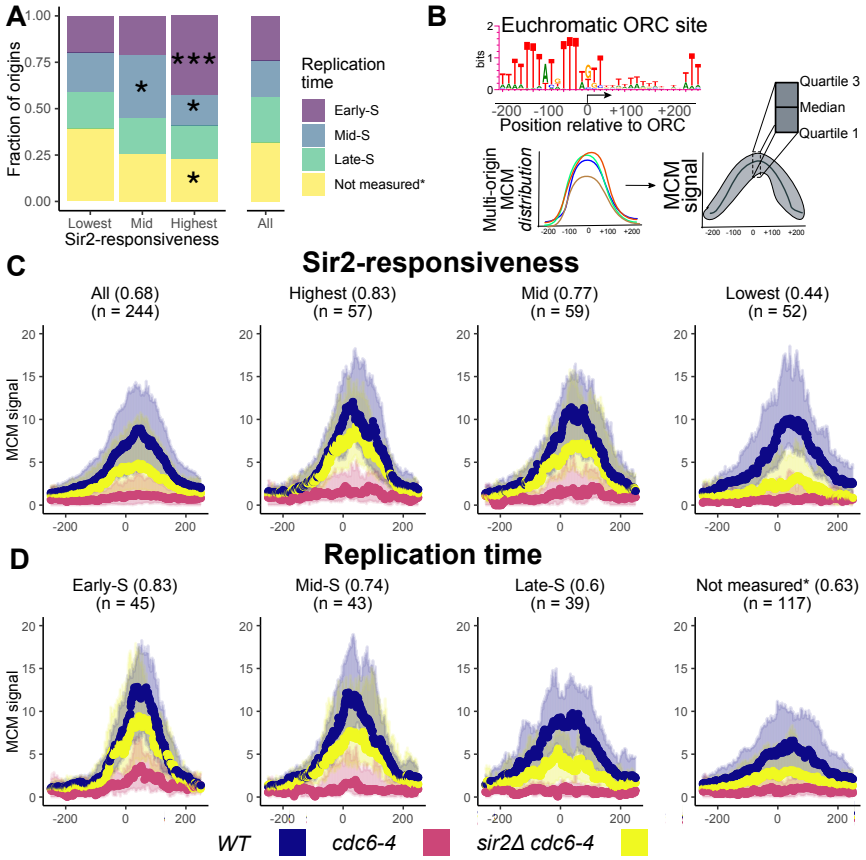

Figure 2: **Early origins were enriched among the euchromatic origins most responsive to *SIR2*. A.** Enrichment of Trep values (n = 312, (Yabuki et al., 2002)) within euchromatic origins parsed by the ability of a *sir2Δ* mutation to rescue MCM ChIP-Seq signals in *cdc6-4* mutant cells cultured at the non-permissive temperature for *cdc6-4* (Hoggard et al., 2018). Origins were parsed into quintiles based on their Sir2-reponsiveness. The Lowest (n=56), Mid (n=61) and Highest (n=62) Sir2-responsive quintiles each contained ˜20% of the euchromatic origins that were assigned a Sir2-responsiveness value. Within each Sir2-responsive group, the fraction of origins with the indicated origin activation times were determined. Hypergeometric distribution was used to compare the enrichments within each Sir2-responsive group relative to the fraction among all origins examined. The P-values for the groups that showed significant enrichment or depletion in each Sir2-responsive group are indicated (*P $\leq$ 0.05; **P $<$ 0.01; ***P $<$ 0.001). **B.** Determining nucleotide-resolution multi-origin MCM distribution of different origin types. MCM ChIP-Seq signals were determined for each nucleotide in each origin fragment oriented with the T-rich start of the ORC binding site on the top strand (position '0'). The final MCM ChIP-Seq signal associated with a given nucleotide was displayed as the median of three biologically independent experiments. To derive the MCM distribution for multiple origins, the per-nucleotide median $\pm$ 1 quartile distribution was calculated and displayed in shaded coloring. **C.** The MCM signal distributions for wild type (*CDC6 SIR2*, dark blue), *cdc6-4* (*cdc6-4 SIR2*, rose), and *cdc6-4 sir2Δ* (yellow) cells were plotted for the indicated Sir2-responsive groups. The number in parenthesis indicates the ratio of MCM signal determined for *cdc6-4 sir2Δ* cells (summed between -100 through +150) to that determined for wild-type cells. The difference in origin numbers used here (n=255) compared to the number used in Figure 1A was the demand in these analyses that origins contained previously annotated match to the ORC binding site (Eaton et al., 2010). **D.** The approach in C was applied to euchromatic origins parsed by their determined replication times in S-phase (Yabuki et al., 2002).

Within euchromatin, Sir2-heterochromatin marks skewed toward early origins.

The molecular hallmarks of Sir2-heterochromatin, namely Sir2-dependent depletion of H4K16ac and Sir3 association with adjacent nucleosomes, are present at euchromatic origins, providing evidence that Sir2 acts directly at euchromatic origins to inhibit MCM complex loading in *cdc6-4* cells (Hoggard et al., 2018). Because early origins were enriched among the most *SIR2*-responsive origins, we asked whether this origin group also showed the highest levels of Sir2-chromatin marks by determining the relative H4K16ac state of origin-adjacent nucleosomes as described previously (see **S3 Figure** for defining the loci used for statistical analysis and **Figure 3A-C**) (Weiner et al., 2015). While all groups of euchromatic origins were flanked by nucleosomes showing relative depletion of H4K16ac compared to a group of euchromatic control loci, early origins showed greater depletion of this Sir2-substrate compared to other groups. The difference was most pronounced at the -1 and +1 nucleosomes, and was *SIR2*-dependent. Additional analysis of nucleosomal H4K16ac levels as well as Sir3 binding were consistent with the conclusion that an early origin was more likely than an origin from another relevant group to show higher levels of Sir2-chromatin features, although there was substantial variability within groups and overlap between groups, consistent with low signals and a stochastic mechanism (**S4 Figure**).

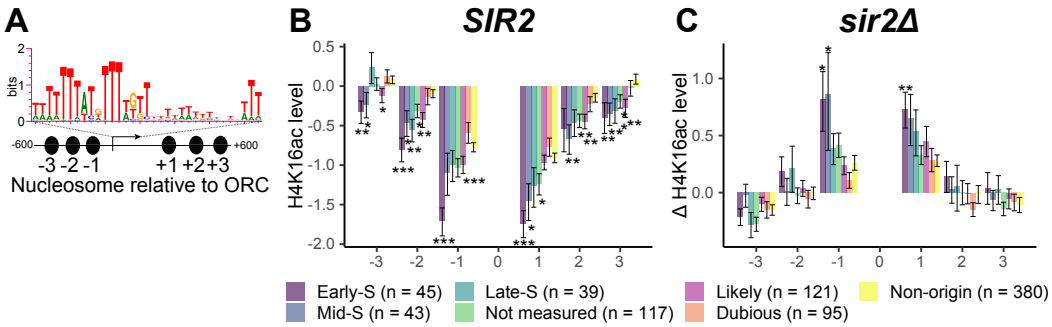

Figure 3: **Sir2-chromatin levels at euchromatic origins.** This diagram depicts the origin-adjacent nucleosomes that were analyzed. **A.** Normalized H4K16ac levels were determined for the nucleosomes in wild type (*SIR2* cells) as described previously (Hoggard et al., 2018). Origins were ranked based on their Trep values and then divided into quintiles, (e.g. Early (20% with lowest Treps), Late (20% with highest Treps)) were examined. Not-measured origins that could not be assigned distinct Trep values were also examined. T-tests were used to compare the means of the H4K16ac signals for each group to the means associated with a random selection of 43 control intergenic euchromatic loci (Hoggard et al., 2018). Likely and Dubious origin groups are as defined in OriDB (Siow et al., 2012). Non-origins are those elements that contain a match to the ORC binding site yet do not show any function as origins (Eaton et al., 2010; Hoggard et al., 2018). P-values meeting various cutoffs are indicated in black and correspond to those in Figure 2.

SIR2 promoted more equitable distribution of MCM complexes between early and late euchromatic origins.

While published data as well as the analyses in **Figure 2** provided evidence that *SIR2* can have a profound effect on MCM complex loading at euchromatic origins in *cdc6-4* cells, the effect of *SIR2* on MCM loading in otherwise wild-type (*CDC6*) cells has not been addressed. Indeed, it is clear that wild type (*CDC6 SIR2*) and *sir2*Δ (*CDC6 sir2*Δ) cells produce similar MCM ChIP-Seq profiles, indicating that any differences that might exist are not obvious (Hoggard et al., 2018). Therefore, we examined this issue using the higher-resolution approach discussed above (**Figure 2B**). In *SIR2* cells, early-, mid- and late- euchromatic origins generated similar MCM signals, while not-measured euchromatic origins generated lower signals, consistent with the high fraction of origins within this group being inefficient (**Figure 4A, S3 Figure**). However, in *sir2*Δ cells the MCM signals for the early- and mid-origin groups were enhanced relative to the late and not-

measured origin groups. We also assessed MCM signals at Sir2-heterochromatic telomeric X-origins (**Figure 4B**). In *SIR2* cells, telomeric X-origins generated similar MCM signals compared to the euchromatic origin groups. However, in *sir2*Δ cells, telomeric X-origins generated MCM signals that were similar to those generated by early- and mid-S-phase origins and greater than those generated by late and not-measured origins. These data provided evidence that Sir2 limited MCM association at both heterochromatic telomeric X-origins and euchromatic early origins relative to late and not-measured euchromatic origins.

To present these data in a more easily quantifiable format, the MCM signals between the -10 and +100 nucleotide positions for each of the fragments within each origin group were summed. The resulting sums were used to assign each origin fragment a Z-score, a measure of how far the MCM signal at that origin varied from the mean behavior of all the origins being assessed. The resulting Z-scores were displayed in box-and-whiskers plots for each origin group (**Figure 4C**). In *SIR2* cells, the median Z-scores of the early- and late-origin groups were slightly different, with the late origin group producing slightly lower MCM Z-scores compared to early origins, consistent with another published MCM ChIP-Seq data set (Das et al., 2015). However, there was substantial overlap of the box plots generated by the early- and late-origin groups, and the differences in MCM Z-scores between these two groups did not meet a P-value cut-off of 0.05. In addition, in *SIR2* cells, telomeric X-origins produced similar MCM Z-scores to each of the euchromatic-origin groups. In contrast, in *sir2*Δ cells, the median Z-score of the early origin group was above the mean score in the population (defined as '0'), and the difference between the median MCM Z-scores generated by the early and late origins was clear, and met a significant P-value cut-off (Wilcoxon Rank Sum test, P [?] 0.01). These data provided evidence that early euchromatic and telomeric X-origins were licensed more efficiently compared to late euchromatic origins in *sir2*Δ cells.

The analyses in **Figure 4C** used origins classified by their Treps but did not account for whether the origin was used efficiently. Thus, some of the origins in these groups might act in only a small fraction of cell cycles. Therefore, to focus on those origins that were most likely to be licensed to similar extents, we repeated the analysis using only those origins within each group that generated an origin efficiency metric in a genome-scale analyses of origin function (McGuffee et al., 2013) (**S1 Figure**). Considering only these efficient origins (i.e. origins that act in most cell cycles and therefore have to be efficiently licensed), the difference between the early and late origin MCM signals observed in *sir2*Δ cells was enhanced. (**Figure 4D**). The telomeric X-origins are missing from this panel because origin function was only reported for one of these origins (McGuffee et al., 2013) (**S1 Figure**). Therefore, within euchromatin, *SIR2* prevents MCM complexes from accumulating at early- relative to late-euchromatic origins, and also attenuates origin licensing at telomeric X-origins. We note that a negative impact of Sir2 on the efficiency of origin licensing at the rDNA origin was not observed, consistent with a recent study (Foss et al., 2019) (**S5 Figure**). Thus, not all origins whose function is inhibited by Sir2-heterochromatin are necessarily inhibited at the MCM complex loading step.

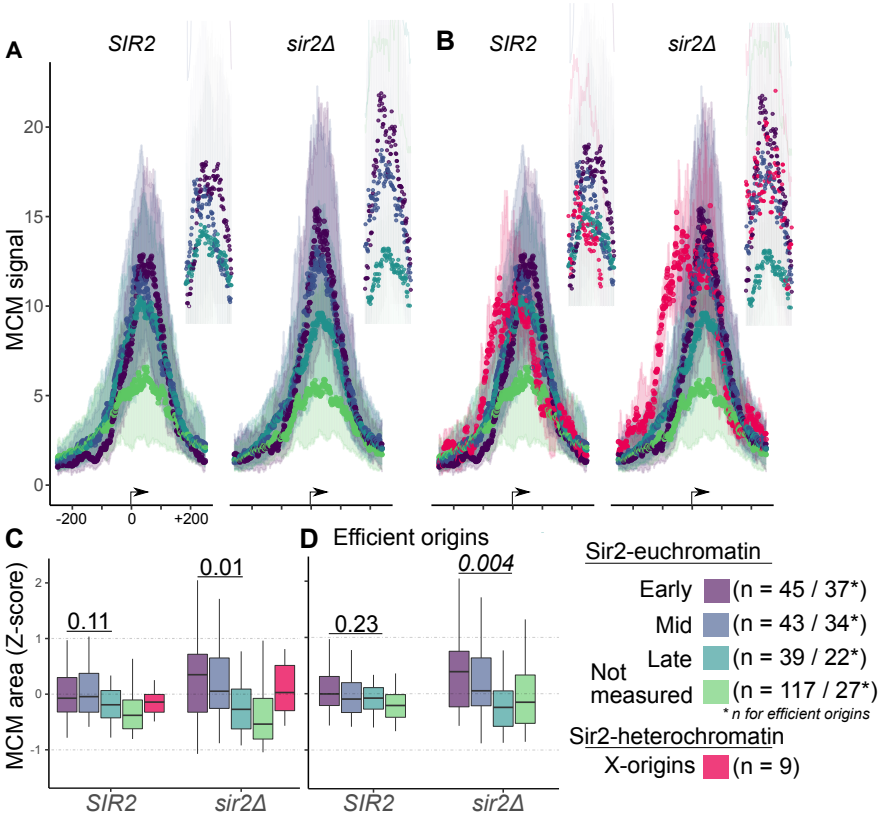

Figure 4: ***SIR2* promoted more equitable distribution of MCM complexes between Early and Late euchromatic origins.** **A.** MCM ChIP-Seq signals were determined as in Figure 2B for the indicated origins in congenic *SIR2* and *sir2Δ* cells. The inset is an expanded view of the data between nucleotides -10 and +100. **B.** Same analyses as in A, except data from the nine telomeric X-origins are included (pink). **C.** The areas (between nucleotides -10 ˜ +100) generated by the scans in B. were determined for each origin within each group and assigned Z-scores and displayed in box-and-whiskers plots. The P-values for the difference between the early and late origin groups' median MCM Z-scores are indicated. The number of origins in each group is indicated in parenthesis prior to the '/' mark. **D.** Same analyses method as in C. except all origins that failed to generate an origin efficiency metric (OEM) in (McGuffee et al., 2013) were removed. The number of origins analyzed in each group is indicated after the '/' and with *. Telomeric X-origins are not shown in this panel because only one X-origin generated an origin efficiency metric. The P-values (Wilcoxon Rank Sum test) for the difference between the early and late origin groups' median MCM Z-scores are indicated.

Relative gains in MCM association correlated with enhanced replication.

The data presented above provided evidence that *SIR2* had an impact on MCM distribution in both *cdc6-4* and *CDC6* cells. To address whether the shift in MCM distribution might impact replication dynamics, S-phase Sort-Seq experiments were performed with the same yeast strains that were used for the MCM ChIP-Seq experiments, except that the cells were cultured at the permissive growth temperature for *cdc6-4* so that the effect of this mutation itself on replication could be examined (**Figure 5 and S6 Figure)** (Müller et al., 2014)**.** Both the *cdc6-4* and *cdc6-4 sir2*Δ mutant cells produced similar chromosome replication profiles to each other that differed from wild type (*CDC6 SIR2*) (**S6 Figure**). This result suggested that the function of many of the same origins was reduced over regions of every chromosome in both *cdc6-4 SIR2* and *cdc6-4*

*sir2*Δ mutant cells relative to wild type cells. To enhance the ability to visualize the replication behavior of origin-containing regions in a more quantifiable format, Sort-Seq signals were assigned to individual 30 kb replicons by calculating the mean value of the normalized Sort-Seq ratios over the entire replicon. These 30 kb replicons were then parsed based on the replication times assigned to their origins as discussed above, and the Sort-Seq signals for each group depicted in box-and-whiskers plots. If this approach accurately depicted S-phase replication dynamics for these regions, then the replicons duplicated by early origins in wild-type cells should produce larger S-phase Sort-Seq signals compared to the replicons duplicated by late origins. We observed this result, indicating that these analyses captured the predicted behavior of replicons based on the Treps of their origins (**Figure 5A**).

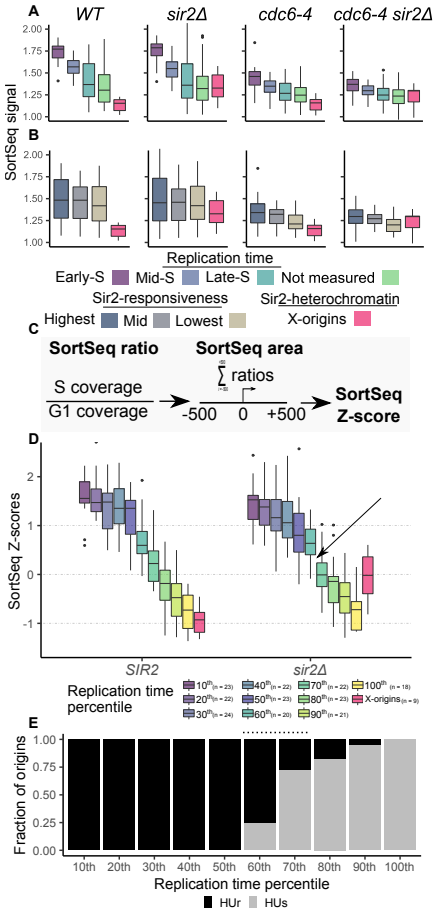

Figure 5: **S-phase Sort-Seq data were used to examine the replication behavior of the indicated regions. A.** Sort-Seq values for 30 kb fragments centered on euchromatic origins parsed by Trep values were depicted in box-and-whisker plots for each of the indicated yeast grown under permissive temperatures for *cdc6-4* (25°C). **B.** As in A except origins were grouped into three different Sir2-responsive groups (see **Figure 2C**), where Sir2-responsiveness is defined by the degree of MCM ChIP-Seq signal rescue in *cdc6-4 sir2Δ* cells as in (Hoggard et al., 2018). **C.** Assigning Sort-Seq Z-scores to distinct origin fragments. **D.** Euchromatic origins parsed by Trep values into ten distinct groups with their Z-scores plotted from the earliest (10th) to the latest (100th) decile in *SIR2* and *sir2Δ* cells. Telomeric X-origin Z-scores are also plotted. **E.** The fraction of hydroxyurea-resistant origins (HUr) and hydroxyurea-sensitive (HUs) was determined for each group in **D.**

Based on these analyses, *SIR2* had no effect on the relative replication dynamics of euchromatin. However, as expected, *SIR2* was required for the normal replication time of Sir2-heterochromatic telomeric X-origins (**Figure 5A**). The expected outcome for telomeric X-origins validated this approach's ability to capture what is known about Sir2-dependent origin function during S-phase. The S-phase Sort-Seq data from the *cdc6-4* and *cdc6-4 sir2*Δ mutant cells generated more compressed replicon distributions in S-phase compared to *CDC6* cells, although the temporal order of replicon duplication was maintained. These data provided evidence that the relative temporal distribution of euchromatic replicon duplication was not substantially altered in *cdc6-4* nor *cdc6-4 sir2*Δ mutant cells, consistent with the observation that the vast majority of rescued MCM complex loading observed in *cdc6-4 sir2*Δ cells occurs at documented DNA replication origins and not at novel sites (Hoggard et al., 2018).

In the *SIR2* and *sir2*Δ cells, the replicons from the three different *SIR2*-responsive groups produced similar broad box-and-whiskers plots using these S-phase Sort-Seq data (**Figure 5B**). This result was not unexpected given that each Sir2-responsive group contained a substantial number of origins from each origin-activation timing group even though the most Sir2-responsive group was enriched for early origins (see **Figure 2A**). However, analysis of the S-phase Sort-Seq data generated by the different *SIR2*-responsive groups in the *cdc6-4* and *cdc6-4 sir2*Δ cells produced a different and notable outcome. In particular, the Sort-Seq values for each group correlated with the alterations in their MCM distribution as observed in **Figure 2C**. Specifically, the group comprised of the euchromatic origins that showed the most substantial *sir2*Δ -mediated rescue of MCM signals (high Sir2-responsive), generated the highest S-phase Sort-Seq values in both *cdc6-4* and *cdc6-4 sir2*Δ cells, while the lowest Sir2-responsive group generated lower Sort-Seq values. Thus, the origin group that most effectively rescued MCM signals in *cdc6-4 sir2*Δ cells (**Figure 2C**) was also the group that showed relatively enhanced replication in an S-phase Sort-Seq experiment. These data provided evidence that the shifted MCM distribution in *cdc6-4 sir2*Δ cells promoted a concomitant shift in replicon function that muted the differences between the discrete timing behaviors of normally temporally distinct euchromatic origin groups.

SIR2 promoted a temporal continuum of euchromatic origin function through S-phase.

While *SIR2* promoted more equitable distribution of MCM complexes across origins (**Figure 4**), the analysis in **Figure 5A** showed no changes in the relative replication behavior of origins, with the exception of telomeric X-origins that advanced their replication time in *sir2*Δ cells, as expected. To examine origin replication timing at greater resolution, we used a more sensitive analytical approach, assigning individual euchromatic origin fragments Z-scores based on their calculated Sort-Seq ratios (**Figure 5C**). The euchromatic origins were then binned into deciles parsed by their Trep values from earliest euchromatic origins (10th percentile) to latest (100th percentile), and the Z-scores in each bin displayed in box-and-whiskers plots (**Figure 5D**). By these analyses, a small but notable gap in euchromatic origin function was revealed between the 60th and 70th Trep percentiles. These data provided evidence that in the absence of *SIR2*, the replication of late euchromatic origins was further delayed relative to early euchromatic origins. Consistent with this interpretation, this gap coincides with the shift of chromosomal origin sensitivity to hydroxyurea, with the vast majority of hydroxyurea-resistant (early) origins residing above the gap and the vast majority of hydroxyurea-sensitive (late) origins residing below the gap (**Figure 5E**).

SIR2 was required for completing replication of late replicating euchromatic origins independent of rDNA replication demands.

Analyses of the S-phase Sort-Seq data above revealed that *SIR2* had a small but noticeable effect on the replication of late euchromatic origins. To further explore this effect and its possible impact, we examined datasets generated from an independent, previously published series of Sort-Seq experiments that included data from early G2 cell populations (Foss et al., 2017). Because these experiments were performed in a

different set of strains from those used here, we first examined the S-phase Sort-Seq datasets generated for this previous study using the Z-score decile approach above. Importantly, the same gap between the 60th and 70th percentiles was observed using this independently generated data set (**S7 Figure**). We then used this data set to analyze the effect *SIR2* had on the extent of euchromatic origin replication in early G2 cell populations, defined as cell populations that had just completed genome duplication based on flow cytometry. The different origin groups produced the expected distinct box-and-whiskers plots in S-phase in both *SIR2* and *sir2*Δ cells characteristic of these groups distinct replication times. However, the *SIR2* and *sir2*Δ cells generated different outcomes in early G2 cell populations (**Figure 6A**). Specifically, in *SIR2* cells, early and late euchromatic origins generated indistinguishable Sort-Seq Z-scores, indicating that both types of origins were completely duplicated by the end of S-phase in all cells in the population, as expected. Only the telomere X-origins had Z-scores below the mean, consistent with the fact that these origins are extremely inefficient and are among the last regions of the genome to be duplicated in wild-type cells. In contrast, in *sir2*Δ cells, the behavior of late and early euchromatic origins skewed away from each other, with the majority of early origin-fragments generating Z-scores above the mean of the population, and the majority of late origin-fragments generating Z-scores below the mean (**Figure 6A**). Thus, in the absence of *SIR2*, a substantial fraction of G2 cells in the population had failed to complete the duplication of late-euchromatic origin fragments. Therefore, *SIR2* was required for complete duplication of late euchromatic origins by the end of S-phase. These analyses provided evidence that in *sir2*Δcells, late euchromatic origins were either substantially delayed for their activation or inactive.

Previous studies establish that *SIR2* has an indirect positive effect on early euchromatic origins that results from its direct repression of the rDNA origin, which is present in hundreds of copies within the yeast rDNA repeat array (Yoshida et al., 2014). In the absence of *SIR2*, the origin within each rDNA repeat (r-ORIGIN) is no longer repressed, such that many more rDNA repeats contain active origins. Thus the rDNA array now sequesters limiting S-phase MCM complex activation factors away from early euchromatic origins, delaying their activation. This effect is proposed to ultimately result in a delay in completing genome duplication of late replicating regions of chromosomes (Foss et al., 2017). In support of this model, *sir2*Δ yeast cells harboring a mutation within the rDNA origin that weakens its function, referred to as *r-origin**, less effectively sequester S-phase MCM complex activation factors. Thus, in *sir2*Δ *r-origin**, more S-phase factors are available, and the *sir2*Δ-dependent under-duplication defect observed for late regions is partially suppressed. We posited that if the relative enhanced licensing of early euchromatic and telomeric origins observed in *sir2*Δ cells were contributing to the delayed duplication of late euchromatic origins, then their delayed duplication measured in early G2 populations would be less sensitive to the *r-origin** compared to telomeric X-origins that had gained MCM complexes. Therefore, we analyzed the early G2 Sort-Seq data in *sir2*Δ cells containing the mutant origin (*sir2*Δ *r-origin**). In *sir2*Δ *r-origin** cells, the delayed duplication of the telomeric X-origin fragments in early G2 was substantially reduced, such that the difference between early euchromatic origins and telomeric X-origins Z-scores in the early G2 sample no longer reached a significant P-value cut-off (**Figure 6A-B**, compare early euchromatic and telomeric X-origins in early G2 in *sir2*Δ *r-ORIGIN* cells to their relative behavior in *sir2*Δ *r-origin** cells). Thus, in the absence of *SIR2* duplication of telomeric X-origins was limited by the availability of S-phase origin activation proteins that were occupied with replicating the rDNA array, consistent with previous published data (Foss et al., 2017). However, many of the late-euchromatic origins remained under duplicated even in the *sir2*Δ *r-origin** cells, particularly when comparing their behavior in wild-type cells (**Figure 6A-B,** compare *sir2*Δ *r-origin** to *SIR2 r-ORIGIN*). Approximately half of the late euchromatic origins remained incompletely duplicated in early G2 cells despite the release of S-phase origin activation factors caused by *r-origin**, consistent with their being under-licensed relative to early euchromatic and telomeric X-origins. We conclude that in *sir2*Δ cells, late-euchromatic origins are the least competitive of all origins for limiting S-phase origin activation proteins because both early euchromatic and telomere-associated origins are sequestering these proteins because of their enhanced levels of licensing. Thus, a major factor delaying the duplication of late euchromatin in *sir2*Δ cells was the shift in MCM complex distribution away from late euchromatic origins.

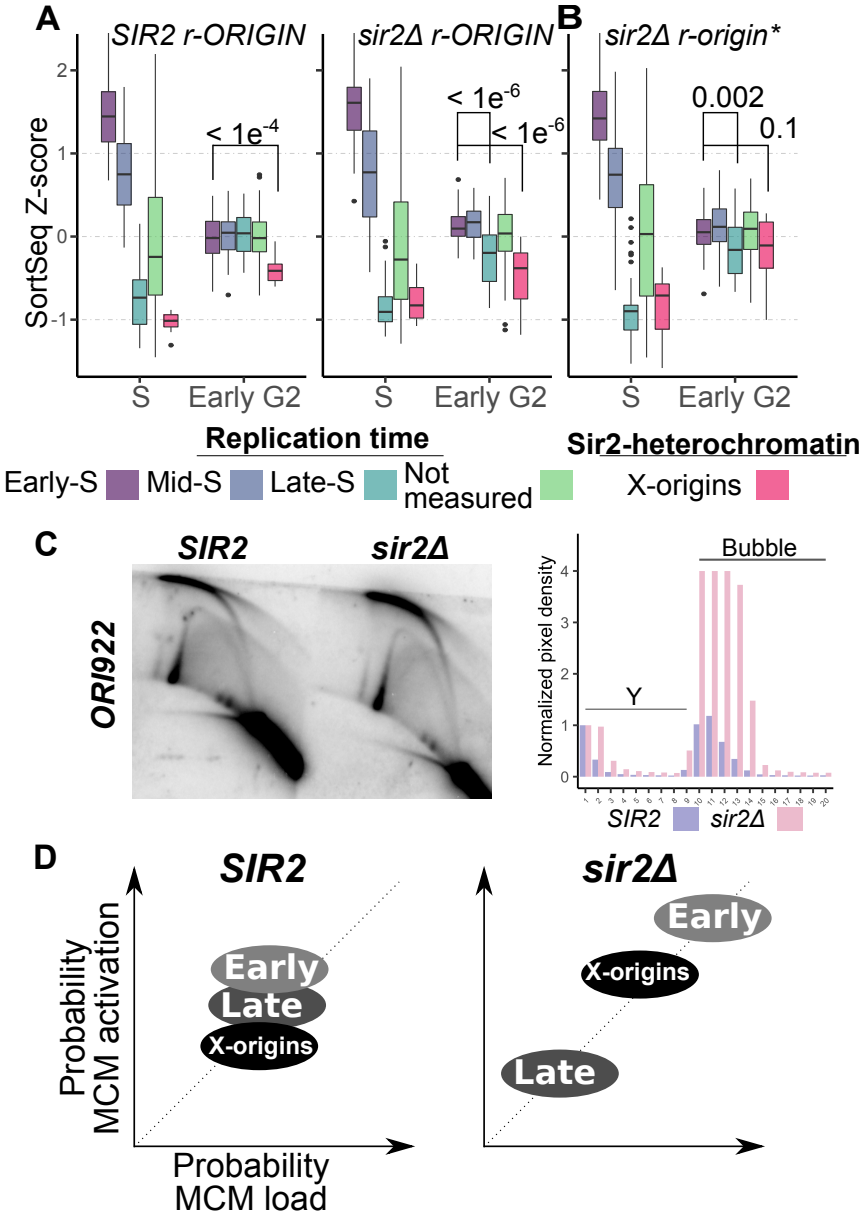

Figure 6: ***SIR2* was required for completing replication of late euchromatic regions independent of rDNA replication demands. A.** Z-scores for the indicated origin fragments from S-phase and early G2-phase *SIR2* and *sir2Δ* cells derived from raw data reported in (Foss et al., 2017) were determined and displayed as box-and-whiskers plots for early-, mid-, and late-euchromatic origins, and heterochromatic telomeric X-origins. **B.** Analyses as in 6A except with data from *sir2Δ r-origin** mutant. **C.** 2-D origin mapping of origin *ORI922* in indicated strains (left panel). Quantitation of these data (right panel). Radioactive intensity generated by the largest replication forks from *SIR2* and *sir2Δ* cells were normalized and assigned a value of 1.0 **D.** Diagram of interpretation of data in this report.

Sir2 limited MCM association and origin function of an early, efficient euchromatic origin, *ORI922*.

The analyses the MCM ChIP-Seq data indicated that *SIR2* prevented early euchromatic origins from gaining MCM signals relative to late euchromatic origins. If these relative gains in MCM signals were indeed due to more cells in the population having effectively licensed these euchromatic origins, then the function of these origins should be enhanced in S-phase. The quantitative analyses of Sort-Seq data indicated that many of these origins generated higher Z-scores in *sir2*Δ cells, consistent with their having acquired enhanced origin function. To challenge this conclusion using an independent origin-specific method we used two-dimensional (2-D) origin mapping to examine the effect of *SIR2* on the chromosomal origin function of euchromatic origin *ORI922* (Friedman and Brewer, 1995) (**Figure 6C** and **S8 Figure**). 2-D origin mapping allows a direct assessment of initiation efficiency by examining the levels of bubble intermediates relative to replication forks. *ORI922* is an early and relatively efficient origin (Origin Efficiency Metric = 0.75 (McGuffee et al., 2013). An OEM of 1.0 is assigned to the most efficient origin in the genome, *ORI305*). We reasoned that *ORI922* had enough capacity to improve in function to allow detection of enhanced efficiency by 2-D origin mapping. As expected, *ORI922*, was an efficient origin in *SIR2* cells. Nevertheless, in *sir2*Δ cells, an enhancement in origin firing of *ORI922* could be detected as an increase in origin bubble relative to replication fork intermediates (**Figure 6C**). Therefore, *SIR2* limited the function of the efficient, early euchromatic origin *ORI922* at the level of MCM complex loading. Thus, the relative gain of MCM signals at early euchromatic origins in *sir2*Δ cells resulted from more cells within the population having effectively licensed these origins.

Discussion

Recent reports establish that the yeast Sir proteins, non-essential repressor proteins best known for their roles in forming heterochromatin domains (a.k.a. transcriptionally silent chromatin), also act directly within euchromatin where they can have an impact on the essential process of chromosomal replication (Gartenberg and Smith, 2016; Hoggard et al., 2018; Puddu et al., 2017). Relevant to this study, we recently reported that Sir2 and Sir3 act directly on the ˜2-4 nucleosomes immediately adjacent to euchromatic DNA replication origins (Hoggard et al., 2018). However, the functional potential of this Sir2-chromatin state in the G1-phase MCM complex loading reaction at chromosomal origins has thus far only been detected in cells in which one of the core origin licensing proteins is defective (e.g. *cdc6-4*, *orc5-1*, *mcm2-1* mutant yeast) (Pappas et al., 2004). In cells with wild-type origin licensing proteins, direct roles for *SIR* genes in MCM complex loading have not been reported. Indeed, MCM ChIP-Seq experiments in *SIR2* and *sir2*Δ cells produce remarkably similar genome-scale MCM binding profiles (Hoggard et al., 2018), suggesting that no major qualitative or quantitative differences in MCM loading at yeast origins is caused by loss of *SIR2*. These data are consistent with the viability of *sir2*Δ cells. Thus, the physiological purpose for Sir2-chromatin at euchromatic origins, despite its genome-wide pervasiveness and its ability to potently inhibit MCM complex loading under mutant conditions, was unknown.

In this report, we addressed this gap in knowledge by undertaking a detailed examination of the effect that *SIR2* had on origin licensing and replication using MCM ChIP-Seq and Sort-Seq data. Sensitive, quantitative computational approaches comparing large numbers of origins parsed by their S-phase activation times provided evidence that early euchromatic origins gained MCM signals relative to late euchromatic origins in *sir2*Δ cells regardless of *CDC6* genotype. Thus Sir2-chromatin attenuated MCM complex loading more effectively at early euchromatic origins compared to late euchromatic origins, consistent with the observation that Sir2-chromatin marks were higher at early euchromatic origins. Because previously reported data establish that Sir2's inhibitory effects on MCM complex loading occur through its catalytic deacetylation of nucleosomes, we propose that the direct repressive properties of this chromatin-state (e.g. compacted nucleosomes, reduced nucleosome mobility) functions directly at individual origins to attenuate MCM complex loading (Pappas et al., 2004; Crampton et al., 2008, Hoggard et al., 2018). Sir2-mediated attenuation of

MCM complex loading at multiple individual origins achieves a physiologically relevant genome-scale impact by skewing replication origin density to early euchromatin at the expense of late euchromatin (**Figure 6D**). The Sir2-chromatin-enforced mechanism to equitably distribute MCM complexes is important for allowing the chromatin-mediated mechanisms that recruit the S-phase origin activation DDK to promote the smooth temporal progression of origin function (Fang et al., 2017; Natsume et al., 2013). If too many MCM complexes are loaded in early replicating euchromatin, the consequence is "hyper-initiation activity" in these regions that ultimately contributes to a delay in duplicating late replicating euchromatin.

Sir2 limited origin licensing at Sir2-heterochromatic telomeric X-origins.

Another important result of this study was the observation that MCM complex loading was limited by Sir2 at telomeric X-origins known to be packaged into Sir2-heterochromatin. While Sir-heterochromatin-mediated inhibition of origin function is an established phenomenon, it has been unclear whether this inhibition occurs at the level of MCM complex loading in G1-phase or access to origin-activation proteins in S-phase or whether both steps are affected (Stevenson and Gottschling, 1999; Yoshida et al., 2014; Palacios DeBeer et al., 2003; Palacios DeBeer and Fox, 1999). The data in this study provided evidence that Sir2 attenuated MCM complex loading at telomeric X-origins substantially, though not completely. Thus, we propose that an important contributing factor to the Sir2-dependent inefficiency of telomeric X-origins, and consequent late replication time of telomeres, is that in a substantial fraction of cells in the population, these elements do not even possess an MCM complex. Indeed, the data provided evidence that telomeric X-origins had a greater intrinsic ability to support MCM complex loading than late euchromatic origins. Thus, the increased probability of telomeric X-origins being licensed compared to late euchromatic origins provided the explanation for how they could more effectively compete for S-phase origin activation factors and complete their duplication prior to late euchromatic origins (**Figure 6D**).

A small, direct molecular effect acting independently and stochastically at many individual origins had an important genome-scale impact for a population of dividing cells.

We initially found two outcomes of this study counterintuitive. First, we would not have predicted that, within euchromatin, Sir2 had a greater negative impact on the function of early compared to late origins. Early euchromatic origins generally exist within the most the most dynamic, transcriptionally active, and open regions of euchromatin, and are adjacent to distinct chromatin-associated proteins that directly recruit proteins that promote origin function (Dion et al., 2007; Fang et al., 2017; Natsume et al., 2013; Miotto et al., 2016). Thus, the discovery that molecular features of Sir2-heterochromatin were greater at these more efficient early euchromatic origins compared to late and inefficient euchromatic origins was hard to reconcile with the paradigmatic view of these repressive heterochromatin regulators. However, we reasoned that the same molecular properties that make early euchromatic origins more receptive and accessible to both the transcriptional and DNA replication machinery might simultaneously make them more accessible to Sir proteins. Indeed, while Sir proteins are concentrated within heterochromatin domains due to their relatively high affinities for Sir-nucleating proteins (e.g. Rap1) and their self-reinforcing cycle of nucleosome modification and binding (Gartenberg and Smith, 2016), even 'stable' heterochromatin is dynamic during the cell cycle, and Sir proteins' interactions with other proteins, like all molecular interactions, have intrinsic on-and-off rates (Aparicio and Gottschling, 1994; Cheng and Gartenberg, 2000). Thus the Sir proteins that are released from heterochromatin have opportunities to sample other regions of the genome. Given the greater dynamics of early euchromatin and ORC's intrinsic affinity for Sir-nucleation within silent regions, it makes sense that the genomic loci these temporarily 'free' proteins might sample most frequently would be the more accessible ORCs bound to early replicating euchromatic regions (Rusche et al., 2003; Fox and McConnell, 2005).

The second initially perplexing outcome was that it was clear from extensive prior investigations and the

data presented here that any Sir2-mediated negative impact at any individual early euchromatic origin had to be quite small. After all, many early euchromatic origins are among the most efficiently used origins in yeast. What possible impact could such a weak level of attenuation of the MCM complex loading reaction at these origins have on yeast biology? The answer comes from considering the issue at the level of multiple individual origins. Consider a single early euchromatic origin with the intrinsic capacity to be licensed with 100% efficiency, but where Sir2-chromatin reduces the probabilty of MCM complex loading by ˜10%. At the level of this individual origin, it would be difficult to envision how such a small effect could be physiologically important. Indeed, while it was gratifying to observe that Sir2 limited the function of the early, efficient euchromatic origin *ORI922*, these data, in the absence of the supporting genomic and genetic results, could have easily been dismissed as biological 'noise' with little relevance to yeast physiology. However, the early replicating regions of the yeast genome contain ˜50 independent origins. While reducing the probability of MCM complex loading by ˜10% at any single one of these origins might have no detectable effect on the fitness of a dividing yeast population, reducing the probability by this amount at each of these 50 individual origins by a similar extent would because it would mean that most cells within the population would be investing resources in replication initiation events within early replicating euchromatin that were not necessary for completing the duplication of these regions. Moreover, this over-investment of licensing in early euchromatin would lead to disrupting the temporal progression of chromosome duplication that allocates replication resources sufficiently to complete duplication of the euchromatic region of the genome by the end of S-phase (Fang et al., 2017; Natsume et al., 2013) . Thus, the stochastic nature of Sir association with many individual efficient, early origins prevents them from achieving their maximal firing efficiency by reducing the probability of MCM complex loading. Notably, an independent study revealed that the highly efficient yeast origin, *ORI416*, was not as efficient as it could be as several nucleotide substitutions within this ORI's control elements enhanced its efficiency (Liachko et al., 2013). Thus, even the most efficient origins are limited in their potential activity possibly by multiple mechanisms. We propose that this limitation is physiologically relevant, and insures that early euchromatin is efficiently replicated without sacrificing the accurate duplication of less active late euchromatic regions.

The attenuating mechanism described in this report has the potential to have a major impact on the fitness of a single-celled organism like yeast through affecting cell proliferation rates as well as genome stability. It is worth noting that the H4K20 histone methylase Set8 maintains a level of chromatin compaction in human tissue culture cells that limits MCM complex loading and promotes genome stability (Shoaib et al., 2018), and that SirT1, the human ortholog of Sir2, limits the activity of dormant origins and promotes genome stability (Utani et al., 2017). Thus, an emerging idea is that the attenuation of origin function on a genome-scale by repressive chromatin modifiers is a conserved feature of eukaryotic chromosome duplication. The high-resolution information about origin positions and functions in *S. cerevisiae* allowed us to show how such an attenuating mechanism promotes the distribution of licensed origins over varying terrains of chromatin. While the importance of origin density and distribution to genome stability has become clear (Alver et al., 2014; Blow et al., 2011; Shima and Pederson, 2017), this is the first study to identify a specific chromatin-mediated mechanism that establishes the spatial distribution of licensed origins across a eukaryotic genome.

Materials and methods

Data analysis All data analyses were performed in R. Scripts that are available upon request.

Yeast Strains The strains used in this study (**Figures 2, 3, S2, S4, S5, 4, S6, 5, 6C**) were congenic derivatives of W303-1A, and were described in detail in (Hoggard et al., 2018). The strains used for the computational analyses in **Figure 6A-B** and **S7 Figure** were described in (Foss et al., 2017).

Sequencing data The raw data used for the experiments in this study have been assigned the following BioProject ID's: PRJNA428768 and PRJNA601998 contain the reads from the MCM ChIP-Seq experiments;

PRJNA601998 contains the reads from the S-phase Sort-Seq experiments (**Figure 5**). The GEO accession GSE90151 contains the reads from the S and G2 Sort-Seq experiments (**Figure 6**).

Identification of ORC-binding-site-containing genomic fragments Multiple studies have identified and annotated ORC binding sites (Eaton et al., 2010; Nieduszynski et al., 2006; Xu et al., 2006). We used the bioinformatics software Mochiview to derive a position specific scoring matrix (PSSM) from all high confidence ORC binding sites (i.e. ORCACS) sequences annotated in (Eaton et al., 2010; Homann and Johnson, 2010) (**S3 Figure**). The ORC site match collection we assembled expanded the collection of sites in (Eaton et al., 2010) to include all likely and dubious origins annotated in OriDB. There were 8523 matches meeting -log10 P-values $\geq$ 4 in the genome (version sacCer3). These matches were mapped to the genome coordinates of all confirmed (n = 410), likely (n = 216) and dubious (n = 203) origins annotated in the OriDB (Siow et al., 2012). In addition, matches were mapped to intergenic spaces (n = 6331) annotated in the Saccharomyces Genome Database (SGD). From the intergenic loci that did not overlap OriDB loci (n = 5224 / 6331), we randomly selected 400 non-origin, ORC site containing loci to use in analyses. When a given locus contained more than one match, the ORC site match with the highest -log10 P value was considered the ORC site match for that locus.

Determining per-nucleotide MCM ChIP-Seq signals and distributions MCM ChIP-Seq experiments were performed on three independent cultures of each indicated strain (three biological independent experiments per strain, except for *cdc6-4*) as described (Hoggard et al., 2018). For each biological independent, reads were mapped to sacCer3 using Bowtie2 and default parameters. Duplicates were marked and removed using MarkDuplicates within Picard tools. Per-nt coverages were determined from mapped, unique reads using Samtool's BedCov. Coverages for each IP and input experiments were normalized for sequencing depth and breadth as outlined previously (Skene and Henikoff, 2015). ChIP/input ratios for each independent culture per strain were mapped to the nucleotides within origin-containing fragments oriented relative to the T-rich ORC site (assigned nucleotide position '0'). Once mapped, the ChIP/input ratio for each nucleotide within each biological replicate was scaled by dividing each ratio by the median IP/input ratio measured between coordinates -600 to -400 relative to the start of the ORC site as described for **Figure 2** . Therefore, each locus within each biological replicate and strain were locally scaled. To derive the per nucleotide MCM ChIP-Seq signal distribution for multiple origins, we determined the per nucleotide median $\pm$ one quartile of the distribution of scaled MCM ChIP/input ratios measured at that nucleotide position for all of the origins within a given group (e.g., Sir2-responsive group, Replication timing group). Thus every nucleotide is represented as a "whisker-less" box-and-whiskers plot for all origins within a group, reflecting the distribution of signal measured within a given group.

Determining H4K16ac levels at nucleosomes adjacent to euchromatic origins Normalized H4K16ac levels at relevant nucleosomes were determined as described previously (Hoggard et al., 2018). Briefly the H4K16ac IP/input ratios for each nucleotide within the coordinates of each nucleosome annotated in (Weiner et al., 2015) were summed. With genome-wide nucleosomal H4K16ac levels thus calculated for every nucleosome in the genome, we mapped the nucleosomes 5' and 3' to the T-rich ORC binding site (nucleosome -3 through nucleosome +3) to 1.2 kb fragments centered and aligned to the start of the T-rich strand of the fragment's ORC binding site. Nucleosomes were also mapped to a control group of loci, 391 randomly selected distinct euchromatic 1.2 kb regions that were not annotated in the OriDB and that lacked an ORCACS match. An arbitrary midpoint was assigned to these control loci and nucleosomes -3 to +3 from this midpoint were mapped. For each control fragment, the mean H4K16ac level for the six nucleosomes was determined (spanning signal), and then the mean of the 391 spanning H4K16ac signals was determined. This value was used to normalize the H4K16ac levels for each nucleosome surrounding the experimental loci (as labeled in **Figure 3B-C**). We also determined the distribution of non-normalized H4K16ac signals and Sir3 levels, as measured by ChIP-Seq, within ordered nucleosomes adjacent to different groups of euchromatic origins (Hoggard et al., 2018; Radman-Livaja et al., 2011; Weiner et al., 2015) (**S4 Figure**).

S-phase Sort-Seq experiments The S-phase Sort-Seq experiments in **Figure 5** were performed as described (Müller et al., 2014).

Calculation of Sort-Seq Z-scores Z-scores were calculated from the sum of normalized Sort-Seq ratios (S / G1 or early G2 / G1) for 1 kbp fragments from unique chromosomal loci. The robustness of the Z-score approach for comparing the relative behavior of independent 1 kb origin fragments within the genome depends on using a large number of 1 kb regions both actively and passively replicated within the population. Therefore, the number of relevant 1 kb regions was maximized by including all unique 1 kb regions outlined in **S3 Figure** (n = 1015) that contained a match to the ORC consensus site, regardless of whether that site corresponded to a functional origin. Additionally, 525 additional loci lacking ORC consensus sites and not overlapping the 1015 fragments with matches were included (non-matched loci). For these loci a midpoint was randomly assigned for centering the 1 kbp fragment. Fragments that contributed to Z-scores were chosen irrespective to presence in euchromatin or heterochromatin.

Two-dimensional origin mapping of *ORI922* was performed as described (Brewer and Fangman, 1987; Fox et al., 1995) with the following alterations: CsCl purified DNA was generated from three liters of yeast growing in liquid YPD at 30°C, and the three pools of gradient-pulled genomic DNA were combined into a single Falcon tube prior to spooling with isopropyl alcohol. This approach was required to recover ˜100 μg genomic DNA per liter of yeast. Three radioactive probes were generated by three separate random labeling reactions (α32P-dCTP) of three distinct gel-purified fragments generated by PCR of yeast genomic DNA. The primer pairs used to generate the *ORI922* probe fragments were: Pair (1) Fwd, TCCTTGGTAG-CAAAGATAAAG, Rev, CTGGGAAACCAAAAGATC; Pair (2) Fwd, TAACATGGGTACAGCAAATC, Rev, TGATCTGAAAAACAGGCA; Pair (3) Fwd, CCGTCCGACATATCATG, Rev, CATTCCCGTCT-GAATAATG. The radioactive blot was exposed to a storage phosphor screen and developed with a Typhoon FLA 9000 phosphor-imager.

Acknowledgments

We are particularly grateful to Melissa Harrison (University of Wisconsin, Madison) for reading and critiquing early drafts of the manuscript, and to Erika Shor (Center for Discovery and Innovation, Hakensack Meridian Health) and members of the Fox lab for many thoughtful conversations. Support for this work was provided by NIHGM056890 to CAF, a Biotechnology and Biological Sciences Research Council grant BB/N016858 to CAM and CAN, and a Wellcome Trust Investigator Award 110064/Z/15/Z to CAN.

References

Alver RC, Chadha GS, Blow JJ. 2014. The contribution of dormant origins to genome stability: from cell biology to human genetics. DNA Repair 19:182–189. doi:10.1016/j.dnarep.2014.03.012

Aparicio OM, Gottschling DE. 1994. Overcoming telomeric silencing: a trans-activator competes to establish gene expression in a cell cycle-dependent way. *Genes Dev* **8**:1133–1146.

Bell SP, Labib K. 2016. Chromosome Duplication in Saccharomyces cerevisiae. *Genetics* **203**:1027–1067.

Bell SP, Stillman B. 1992. ATP-dependent recognition of eukaryotic origins of DNA replication by a multi-protein complex. *Nature* **357**:128–134.

Blow JJ, Ge XQ, Jackson DA. 2011. How dormant origins promote complete genome replication. *Trends Biochem Sci* **36**:405–414. doi:10.1016/j.tibs.2011.05.002

Cheng T-H, Gartenberg MR. 2000. Yeast heterochromatin is a dynamic structure that requires silencers continuously. *Genes Dev* **14**:452–463.

Crampton A, Chang F, Pappas DLJ, Frisch RL, Weinreich M. 2008. An ARS element inhibits DNA replication through a SIR2-dependent mechanism. *Mol Cell* **30**:156–166.

Das SP, Borrman T, Liu VW, Yang SC-H, Bechhoefer J, Rhind N. 2015. Replication timing is regulated by the number of MCMs loaded at origins. *Genome Res* **25**:1886–1892.

Debatisse M, Le Tallec B, Letessier A, Dutrillaux B, Brison O. 2012. Common fragile sites: mechanisms of instability revisited. *Trends Genet* **28**:22–32.

Dion MF, Kaplan T, Kim M, Buratowski S, Friedman N, Rando OJ. 2007. Dynamics of replication-independent histone turnover in budding yeast. *Science* **315**:1405–1408.

Eaton ML, Galani K, Kang S, Bell SP, MacAlpine DM. 2010. Conserved nucleosome positioning defines replication origins. *Genes Dev* **24**:748–753.

Fang D, Lengronne A, Shi D, Forey R, Skrzypczak M, Ginalski K, Yan C, Wang X, Cao Q, Pasero P, Lou H. 2017. Dbf4 recruitment by forkhead transcription factors defines an upstream rate-limiting step in determining origin firing timing. *Genes Dev* **31**:2405–2415.

Feng W, Collingwood D, Boeck ME, Fox LA, Alvino GM, Fangman WL, Raghuraman MK, Brewer BJ. 2006. Genomic mapping of single-stranded DNA in hydroxyurea-challenged yeasts identifies origins of replication. *Nat Cell Biol* **8**:148–155.

Foss EJ, Gatbonton-Schwager T, Thiesen AH, Taylor E, Soriano R, Lao U, MacAlpine DM, Bedalov A. 2019. Sir2 suppresses transcription-mediated displacement of Mcm2-7 replicative helicases at the ribosomal DNA repeats. *PLoS Genet* **15**:e1008138. doi:10.1371/journal.pgen.1008138

Foss EJ, Lao U, Dalrymple E, Adrianse RL, Loe T, Bedalov A. 2017. SIR2 suppresses replication gaps and genome instability by balancing replication between repetitive and unique sequences. *Proc Natl Acad Sci U A* **114**:552–557.

Fox CA, Loo S, Dillin A, Rine J. 1995. The origin recognition complex has essential functions in transcriptional silencing and chromosomal replication. *Genes Dev* **9**:911–924.

Fox CA, McConnell KH. 2005. Toward biochemical understanding of a transcriptionally silenced chromosomal domain in Saccharomyces cerevisiae. *J Biol Chem* **280**:8629–8632.

Friedman KL, Brewer BJ. 1995. Analysis of replication intermediates by two-dimensional agarose gel electrophoresis. *Methods Enzym* **262**:613–627.

Gartenberg MR, Smith JS. 2016. The Nuts and Bolts of Transcriptionally Silent Chromatin in Saccharomyces cerevisiae. *Genetics* **203**:1563–1599.

Gros J, Kumar C, Lynch G, Yadav T, Whitehouse I, Remus D. 2015. Post-licensing Specification of Eukaryotic Replication Origins by Facilitated Mcm2-7 Sliding along DNA. *Mol Cell* **60**:797–807.

Hoggard T, Shor E, Muller CA, Nieduszynski CA, Fox CA. 2013. A Link between ORC-origin binding mechanisms and origin activation time revealed in budding yeast. *PLoS Genet* **9**:e1003798.

Hoggard TA, Chang F, Perry KR, Subramanian S, Kenworthy J, Chueng J, Shor E, Hyland EM, Boeke JD, Weinreich M, Fox CA. 2018. Yeast heterochromatin regulators Sir2 and Sir3 act directly at euchromatic DNA replication origins. *PLoS Genet* **14**:e1007418.

Homann OR, Johnson AD. 2010. MochiView: versatile software for genome browsing and DNA motif analysis. *BMC Biol* **8**:49.

Knott SR, Peace JM, Ostrow AZ, Gan Y, Rex AE, Viggiani CJ, Tavare S, Aparicio OM. 2012. Forkhead transcription factors establish origin timing and long-range clustering in S. cerevisiae. *Cell* **148**:99–111.

Kwan EX, Foss EJ, Tsuchiyama S, Alvino GM, Kruglyak L, Kaeberlein M, Raghuraman MK, Brewer BJ, Kennedy BK, Bedalov A. 2013. A Natural Polymorphism in rDNA Replication Origins Links Origin Activation with Calorie Restriction and Lifespan. *PLoS Genet* **9**:e1003329.

Letessier A, Millot GA, Koundrioukoff S, Lachages A-M, Vogt N, Hansen RS, Malfoy B, Brison O, Debatisse M. 2011. Cell-type-specific replication initiation programs set fragility of the FRA3B fragile site. *Nature* **470**:120–123.

Liachko I, Youngblood RA, Keich U, Dunham MJ. 2013. High-resolution mapping, characterization, and optimization of autonomously replicating sequences in yeast. *Genome Res* **23**:698–704.

Mantiero D, Mackenzie A, Donaldson A, Zegerman P. 2011. Limiting replication initiation factors execute the temporal programme of origin firing in budding yeast. *Embo J* **30**:4805–4814.

McGuffee SR, Smith DJ, Whitehouse I. 2013. Quantitative, genome-wide analysis of eukaryotic replication initiation and termination. *Mol Cell* **50**:123–135. doi:10.1016/j.molcel.2013.03.004

Miotto B, Ji Z, Struhl K. 2016. Selectivity of ORC binding sites and the relation to replication timing, fragile sites, and deletions in cancers. *Proc Natl Acad Sci U A* **113**:E4810–9.

Müller CA, Hawkins M, Retkute R, Malla S, Wilson R, Blythe MJ, Nakato R, Komata M, Shirahige K, de Moura AP, Nieduszynski CA. 2014. The dynamics of genome replication using deep sequencing. *Nucleic Acids Res* **42**:e3–e3.

Müller CA, Nieduszynski CA. 2017. DNA replication timing influences gene expression level. *J Cell Biol* **216**:1907–1914.

Muller P, Park S, Shor E, Huebert DJ, Warren CL, Ansari AZ, Weinreich M, Eaton ML, MacAlpine DM, Fox CA. 2010. The conserved bromo-adjacent homology domain of yeast Orc1 functions in the selection of DNA replication origins within chromatin. *Genes Dev* **24**:1418–1433.

Natsume T, Muller CA, Katou Y, Retkute R, Gierlinski M, Araki H, Blow JJ, Shirahige K, Nieduszynski CA, Tanaka TU. 2013. Kinetochores coordinate pericentromeric cohesion and early DNA replication by Cdc7-Dbf4 kinase recruitment. *Mol Cell* **50**:661–674.

Newman TJ, Mamun MA, Nieduszynski CA, Blow JJ. 2013. Replisome stall events have shaped the distribution of replication origins in the genomes of yeasts. *Nucleic Acids Res* **41**:9705–9718.

Nieduszynski CA, Knox Y, Donaldson AD. 2006. Genome-wide identification of replication origins in yeast by comparative genomics. *Genes Dev* **20**:1874–1879.

Palacios DeBeer MA, Fox CA. 1999. A role for a replicator dominance mechanism in silencing. *Embo J* **18**:3808–3819.

Palacios DeBeer MA, Muller U, Fox CA. 2003. Differential DNA affinity specifies roles for the origin recognition complex in budding yeast heterochromatin. *Genes Dev* **17**:1817–1822.

Pappas DLJ, Frisch R, Weinreich M. 2004. The NAD(+)-dependent Sir2p histone deacetylase is a negative regulator of chromosomal DNA replication. *Genes Dev* **18**:769–781.

Peterman N, Levine E. 2016. Sort-seq under the hood: implications of design choices on large-scale characterization of sequence-function relations. *BMC Genomics* **17**:206. doi:10.1186/s12864-016-2533-5

Pohl TJ, Brewer BJ, Raghuraman MK. 2012. Functional Centromeres Determine the Activation Time of Pericentric Origins of DNA Replication in Saccharomyces cerevisiae. *PLoS Genet* **8**:e1002677.

Puddu F, Salguero I, Herzog M, Geisler NJ, Costanzo V, Jackson SP. 2017. Chromatin determinants impart camptothecin sensitivity. *EMBO Rep* **18**:1000–1012. doi:10.15252/embr.201643560

Radman-Livaja M, Ruben G, Weiner A, Friedman N, Kamakaka R, Rando OJ. 2011. Dynamics of Sir3 spreading in budding yeast: secondary recruitment sites and euchromatic localization. *Embo J* **30**:1012–1026.

Raghuraman MK, Winzeler EA, Collingwood D, Hunt S, Wodicka L, Conway A, Lockhart DJ, Davis RW, Brewer BJ, Fangman WL. 2001. Replication dynamics of the yeast genome. *Science* **294**:115–121.

Rusche LN, Kirchmaier AL, Rine J. 2003. The establishment, inheritance, and function of silenced chromatin in Saccharomyces cerevisiae. *Annu Rev Biochem* **72**:481–516.

Shima N, Pederson KD. 2017. Dormant origins as a built-in safeguard in eukaryotic DNA replication against genome instability and disease development. *DNA Repair* **56**:166–173. doi:10.1016/j.dnarep.2017.06.019

Shoaib M, Walter D, Gillespie PJ, Izard F, Fahrenkrog B, Lleres D, Lerdrup M, Johansen JV, Hansen K, Julien E, Blow JJ, Sørensen CS. 2018. Histone H4K20 methylation mediated chromatin compaction threshold ensures genome integrity by limiting DNA replication licensing. *Nat Commun* **9**:3704. doi:10.1038/s41467-018-06066-8

Siow CC, Nieduszynska SR, Muller CA, Nieduszynski CA. 2012. OriDB, the DNA replication origin database updated and extended. *Nucleic Acids Res* **40**:D682–6.

Stevenson JB, Gottschling DE. 1999. Telomeric chromatin modulates replication timing near chromosome ends. *Genes Dev* **13**:146–151.

Tanaka S, Nakato R, Katou Y, Shirahige K, Araki H. 2011. Origin association of Sld3, Sld7, and Cdc45 proteins is a key step for determination of origin-firing timing. *Curr Biol* **21**:2055–2063.

Utani K, Fu H, Jang S-M, Marks AB, Smith OK, Zhang Y, Redon CE, Shimizu N, Aladjem MI. 2017. Phosphorylated SIRT1 associates with replication origins to prevent excess replication initiation and preserve genomic stability. *Nucleic Acids Res* **45**:7807–7824.

van Brabant AJ, Buchanan CD, Charboneau E, Fangman WL, Brewer BJ. 2001. An origin-deficient yeast artificial chromosome triggers a cell cycle checkpoint. *Mol Cell* **7**:705–713.

Weiner A, Hsieh T-HS, Appleboim A, Chen HV, Rahat A, Amit I, Rando OJ, Friedman N. 2015. High-Resolution Chromatin Dynamics during a Yeast Stress Response. *Mol Cell* **58**:371–386.

Wyrick JJ, Aparicio JG, Chen T, Barnett JD, Jennings EG, Young RA, Bell SP, Aparicio OM. 2001. Genome-wide distribution of ORC and MCM proteins in S. cerevisiae: high-resolution mapping of replication origins. *Science* **294**:2357–2360.

Xu W, Aparicio JG, Aparicio OM, Tavare S. 2006. Genome-wide mapping of ORC and Mcm2p binding sites on tiling arrays and identification of essential ARS consensus sequences in S. cerevisiae. *BMC Genomics* **7**:276.

Yabuki N, Terashima H, Kitada K. 2002. Mapping of early firing origins on a replication profile of budding yeast. *Genes Cells* **7**:781–789.

Yoshida K, Bacal J, Desmarais D, Padioleau I, Tsaponina O, Chabes A, Pantesco V, Dubois E, Parrinello H, Skrzypczak M, Ginalski K, Lengronne A, Pasero P. 2014. The Histone Deacetylases Sir2 and Rpd3 Act on Ribosomal DNA to Control the Replication Program in Budding Yeast. *Mol Cell* **54**:691–697.

Alver RC, Chadha GS, Blow JJ. 2014. The contribution of dormant origins to genome stability: from cell biology to human genetics. DNA Repair 19:182–189. doi:10.1016/j.dnarep.2014.03.012

Aparicio OM, Gottschling DE. 1994. Overcoming telomeric silencing: a trans-activator competes to establish gene expression in a cell cycle-dependent way. *Genes Dev* **8**:1133–1146.

Bell SP, Labib K. 2016. Chromosome Duplication in Saccharomyces cerevisiae. *Genetics* **203**:1027–1067.

Bell SP, Stillman B. 1992. ATP-dependent recognition of eukaryotic origins of DNA replication by a multiprotein complex. *Nature* **357**:128–134.

Blow JJ, Ge XQ, Jackson DA. 2011. How dormant origins promote complete genome replication. *Trends Biochem Sci* **36**:405–414. doi:10.1016/j.tibs.2011.05.002

Cheng T-H, Gartenberg MR. 2000. Yeast heterochromatin is a dynamic structure that requires silencers continuously. *Genes Dev* **14**:452–463.

Crampton A, Chang F, Pappas DLJ, Frisch RL, Weinreich M. 2008. An ARS element inhibits DNA replication through a SIR2-dependent mechanism. *Mol Cell* **30**:156–166.

Das SP, Borrman T, Liu VW, Yang SC-H, Bechhoefer J, Rhind N. 2015. Replication timing is regulated by the number of MCMs loaded at origins. *Genome Res* **25**:1886–1892.

Debatisse M, Le Tallec B, Letessier A, Dutrillaux B, Brison O. 2012. Common fragile sites: mechanisms of instability revisited. *Trends Genet* **28**:22–32.

Dion MF, Kaplan T, Kim M, Buratowski S, Friedman N, Rando OJ. 2007. Dynamics of replication-independent histone turnover in budding yeast. *Science* **315**:1405–1408.

Eaton ML, Galani K, Kang S, Bell SP, MacAlpine DM. 2010. Conserved nucleosome positioning defines replication origins. *Genes Dev* **24**:748–753.

Fang D, Lengronne A, Shi D, Forey R, Skrzypczak M, Ginalski K, Yan C, Wang X, Cao Q, Pasero P, Lou H. 2017. Dbf4 recruitment by forkhead transcription factors defines an upstream rate-limiting step in determining origin firing timing. *Genes Dev* **31**:2405–2415.

Feng W, Collingwood D, Boeck ME, Fox LA, Alvino GM, Fangman WL, Raghuraman MK, Brewer BJ. 2006. Genomic mapping of single-stranded DNA in hydroxyurea-challenged yeasts identifies origins of replication. *Nat Cell Biol* **8**:148–155.

Foss EJ, Gatbonton-Schwager T, Thiesen AH, Taylor E, Soriano R, Lao U, MacAlpine DM, Bedalov A. 2019. Sir2 suppresses transcription-mediated displacement of Mcm2-7 replicative helicases at the ribosomal DNA repeats. *PLoS Genet* **15**:e1008138. doi:10.1371/journal.pgen.1008138

Foss EJ, Lao U, Dalrymple E, Adrianse RL, Loe T, Bedalov A. 2017. SIR2 suppresses replication gaps and genome instability by balancing replication between repetitive and unique sequences. *Proc Natl Acad Sci U A* **114**:552–557.

Fox CA, Loo S, Dillin A, Rine J. 1995. The origin recognition complex has essential functions in transcriptional silencing and chromosomal replication. *Genes Dev* **9**:911–924.

Fox CA, McConnell KH. 2005. Toward biochemical understanding of a transcriptionally silenced chromosomal domain in Saccharomyces cerevisiae. *J Biol Chem* **280**:8629–8632.

Friedman KL, Brewer BJ. 1995. Analysis of replication intermediates by two-dimensional agarose gel electrophoresis. *Methods Enzym* **262**:613–627.

Gartenberg MR, Smith JS. 2016. The Nuts and Bolts of Transcriptionally Silent Chromatin in Saccharomyces cerevisiae. *Genetics* **203**:1563–1599.

Gros J, Kumar C, Lynch G, Yadav T, Whitehouse I, Remus D. 2015. Post-licensing Specification of Eukaryotic Replication Origins by Facilitated Mcm2-7 Sliding along DNA. *Mol Cell* **60**:797–807.

Hoggard T, Shor E, Muller CA, Nieduszynski CA, Fox CA. 2013. A Link between ORC-origin binding mechanisms and origin activation time revealed in budding yeast. *PLoS Genet* **9**:e1003798.

Hoggard TA, Chang F, Perry KR, Subramanian S, Kenworthy J, Chueng J, Shor E, Hyland EM, Boeke JD, Weinreich M, Fox CA. 2018. Yeast heterochromatin regulators Sir2 and Sir3 act directly at euchromatic

DNA replication origins. *PLoS Genet* **14**:e1007418.

Homann OR, Johnson AD. 2010. MochiView: versatile software for genome browsing and DNA motif analysis. *BMC Biol* **8**:49.

Knott SR, Peace JM, Ostrow AZ, Gan Y, Rex AE, Viggiani CJ, Tavare S, Aparicio OM. 2012. Forkhead transcription factors establish origin timing and long-range clustering in S. cerevisiae. *Cell* **148**:99–111.

Kwan EX, Foss EJ, Tsuchiyama S, Alvino GM, Kruglyak L, Kaeberlein M, Raghuraman MK, Brewer BJ, Kennedy BK, Bedalov A. 2013. A Natural Polymorphism in rDNA Replication Origins Links Origin Activation with Calorie Restriction and Lifespan. *PLoS Genet* **9**:e1003329.

Letessier A, Millot GA, Koundrioukoff S, Lachages A-M, Vogt N, Hansen RS, Malfoy B, Brison O, Debatisse M. 2011. Cell-type-specific replication initiation programs set fragility of the FRA3B fragile site. *Nature* **470**:120–123.

Liachko I, Youngblood RA, Keich U, Dunham MJ. 2013. High-resolution mapping, characterization, and optimization of autonomously replicating sequences in yeast. *Genome Res* **23**:698–704.

Mantiero D, Mackenzie A, Donaldson A, Zegerman P. 2011. Limiting replication initiation factors execute the temporal programme of origin firing in budding yeast. *Embo J* **30**:4805–4814.

McGuffee SR, Smith DJ, Whitehouse I. 2013. Quantitative, genome-wide analysis of eukaryotic replication initiation and termination. *Mol Cell* **50**:123–135. doi:10.1016/j.molcel.2013.03.004

Miotto B, Ji Z, Struhl K. 2016. Selectivity of ORC binding sites and the relation to replication timing, fragile sites, and deletions in cancers. *Proc Natl Acad Sci U A* **113**:E4810–9.

Müller CA, Hawkins M, Retkute R, Malla S, Wilson R, Blythe MJ, Nakato R, Komata M, Shirahige K, de Moura AP, Nieduszynski CA. 2014. The dynamics of genome replication using deep sequencing. *Nucleic Acids Res* **42**:e3–e3.

Müller CA, Nieduszynski CA. 2017. DNA replication timing influences gene expression level. *J Cell Biol* **216**:1907–1914.

Muller P, Park S, Shor E, Huebert DJ, Warren CL, Ansari AZ, Weinreich M, Eaton ML, MacAlpine DM, Fox CA. 2010. The conserved bromo-adjacent homology domain of yeast Orc1 functions in the selection of DNA replication origins within chromatin. *Genes Dev* **24**:1418–1433.

Natsume T, Muller CA, Katou Y, Retkute R, Gierlinski M, Araki H, Blow JJ, Shirahige K, Nieduszynski CA, Tanaka TU. 2013. Kinetochores coordinate pericentromeric cohesion and early DNA replication by Cdc7-Dbf4 kinase recruitment. *Mol Cell* **50**:661–674.

Newman TJ, Mamun MA, Nieduszynski CA, Blow JJ. 2013. Replisome stall events have shaped the distribution of replication origins in the genomes of yeasts. *Nucleic Acids Res* **41**:9705–9718.

Nieduszynski CA, Knox Y, Donaldson AD. 2006. Genome-wide identification of replication origins in yeast by comparative genomics. *Genes Dev* **20**:1874–1879.

Palacios DeBeer MA, Fox CA. 1999. A role for a replicator dominance mechanism in silencing. *Embo J* **18**:3808–3819.

Palacios DeBeer MA, Muller U, Fox CA. 2003. Differential DNA affinity specifies roles for the origin recognition complex in budding yeast heterochromatin. *Genes Dev* **17**:1817–1822.

Pappas DLJ, Frisch R, Weinreich M. 2004. The NAD(+)-dependent Sir2p histone deacetylase is a negative regulator of chromosomal DNA replication. *Genes Dev* **18**:769–781.

Peterman N, Levine E. 2016. Sort-seq under the hood: implications of design choices on large-scale characterization of sequence-function relations. *BMC Genomics* **17**:206. doi:10.1186/s12864-016-2533-5

Pohl TJ, Brewer BJ, Raghuraman MK. 2012. Functional Centromeres Determine the Activation Time of Pericentric Origins of DNA Replication in Saccharomyces cerevisiae. *PLoS Genet* **8**:e1002677.

Puddu F, Salguero I, Herzog M, Geisler NJ, Costanzo V, Jackson SP. 2017. Chromatin determinants impart camptothecin sensitivity. *EMBO Rep* **18**:1000–1012. doi:10.15252/embr.201643560

Radman-Livaja M, Ruben G, Weiner A, Friedman N, Kamakaka R, Rando OJ. 2011. Dynamics of Sir3 spreading in budding yeast: secondary recruitment sites and euchromatic localization. *Embo J* **30**:1012–1026.

Raghuraman MK, Winzeler EA, Collingwood D, Hunt S, Wodicka L, Conway A, Lockhart DJ, Davis RW, Brewer BJ, Fangman WL. 2001. Replication dynamics of the yeast genome. *Science* **294**:115–121.

Rusche LN, Kirchmaier AL, Rine J. 2003. The establishment, inheritance, and function of silenced chromatin in Saccharomyces cerevisiae. *Annu Rev Biochem* **72**:481–516.

Shima N, Pederson KD. 2017. Dormant origins as a built-in safeguard in eukaryotic DNA replication against genome instability and disease development. *DNA Repair* **56**:166–173. doi:10.1016/j.dnarep.2017.06.019

Shoaib M, Walter D, Gillespie PJ, Izard F, Fahrenkrog B, Lleres D, Lerdrup M, Johansen JV, Hansen K, Julien E, Blow JJ, Sørensen CS. 2018. Histone H4K20 methylation mediated chromatin compaction threshold ensures genome integrity by limiting DNA replication licensing. *Nat Commun* **9**:3704. doi:10.1038/s41467-018-06066-8

Siow CC, Nieduszynska SR, Muller CA, Nieduszynski CA. 2012. OriDB, the DNA replication origin database updated and extended. *Nucleic Acids Res* **40**:D682–6.

Stevenson JB, Gottschling DE. 1999. Telomeric chromatin modulates replication timing near chromosome ends. *Genes Dev* **13**:146–151.

Tanaka S, Nakato R, Katou Y, Shirahige K, Araki H. 2011. Origin association of Sld3, Sld7, and Cdc45 proteins is a key step for determination of origin-firing timing. *Curr Biol* **21**:2055–2063.

Utani K, Fu H, Jang S-M, Marks AB, Smith OK, Zhang Y, Redon CE, Shimizu N, Aladjem MI. 2017. Phosphorylated SIRT1 associates with replication origins to prevent excess replication initiation and preserve genomic stability. *Nucleic Acids Res* **45**:7807–7824.

van Brabant AJ, Buchanan CD, Charboneau E, Fangman WL, Brewer BJ. 2001. An origin-deficient yeast artificial chromosome triggers a cell cycle checkpoint. *Mol Cell* **7**:705–713.

Weiner A, Hsieh T-HS, Appleboim A, Chen HV, Rahat A, Amit I, Rando OJ, Friedman N. 2015. High-Resolution Chromatin Dynamics during a Yeast Stress Response. *Mol Cell* **58**:371–386.

Wyrick JJ, Aparicio JG, Chen T, Barnett JD, Jennings EG, Young RA, Bell SP, Aparicio OM. 2001. Genome-wide distribution of ORC and MCM proteins in S. cerevisiae: high-resolution mapping of replication origins. *Science* **294**:2357–2360.

Xu W, Aparicio JG, Aparicio OM, Tavare S. 2006. Genome-wide mapping of ORC and Mcm2p binding sites on tiling arrays and identification of essential ARS consensus sequences in S. cerevisiae. *BMC Genomics* **7**:276.

Yabuki N, Terashima H, Kitada K. 2002. Mapping of early firing origins on a replication profile of budding yeast. *Genes Cells* **7**:781–789.

Yoshida K, Bacal J, Desmarais D, Padioleau I, Tsaponina O, Chabes A, Pantesco V, Dubois E, Parrinello H, Skrzypczak M, Ginalski K, Lengronne A, Pasero P. 2014. The Histone Deacetylases Sir2 and Rpd3 Act on Ribosomal DNA to Control the Replication Program in Budding Yeast. *Mol Cell* **54**:691–697.

Supplementary Material

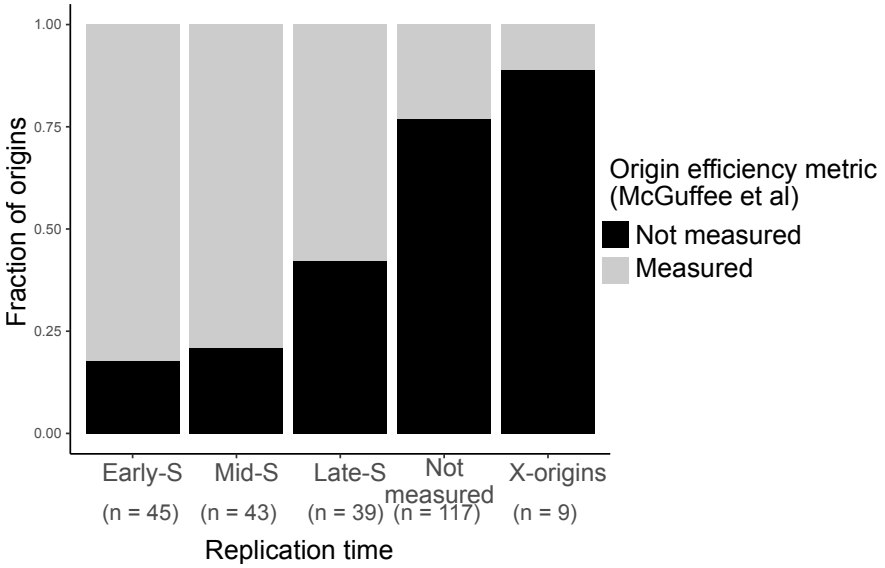

Figure S1: **The majority of early- and mid-S origins are efficient origins, while the majority of not-measured origins are inefficient.** The fraction of euchromatic origins assigned Treps within the indicated ranges that also generated an origin efficiency value by genome-scale replication-initiation point mapping (McGuffee et al., 2013; Yabuki et al., 2002).

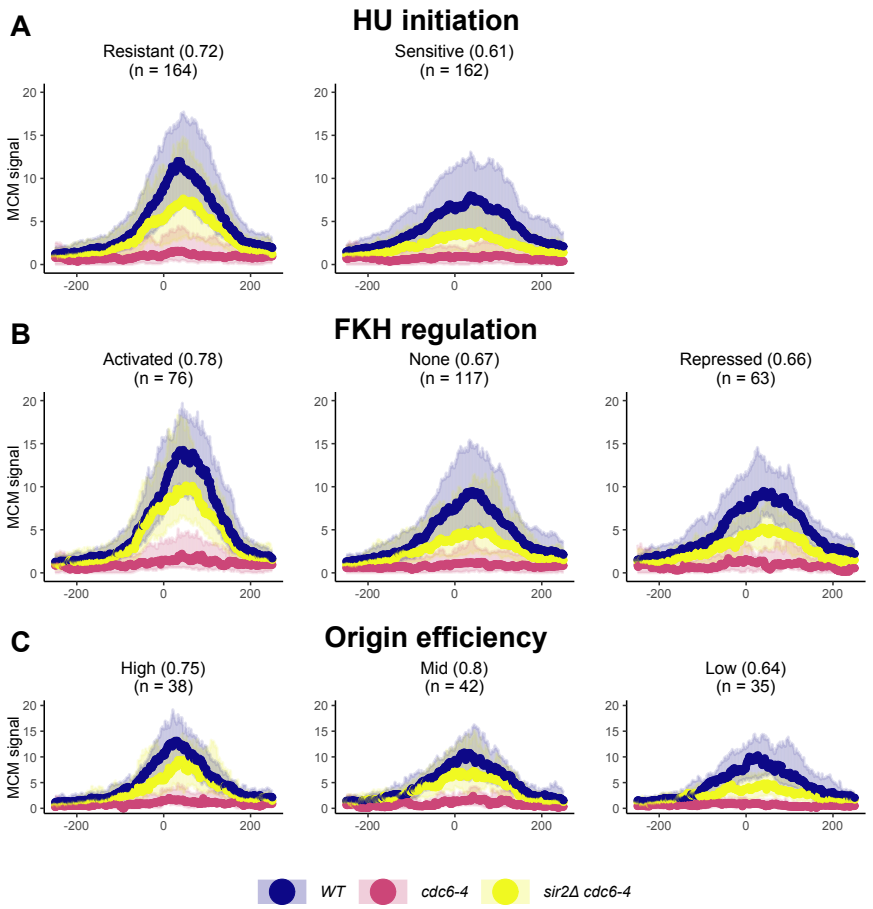

Figure S2: **Euchromatic origins parsed by additional measures of origin function. A.** Origins were parsed based on their sensitivity to the ribonucleotide reductase inhibitor hydroxyurea (HU). Origins that normally function in first half of S-phase are typically resistant to HU, meaning that when cells are released from G1 arrest in the presence of HU, they fire. However, origins that function in the last half of S-phase are sensitive to HU, meaning that under the same experimental conditions they fail to fire. **B.** Origins parsed by their regulation by Fkh1/2 (Knott et al., 2012). FKH activated origins are normally activated early in S-phase while FKH repressed are normally activated late in S-phase. **C.** Origins parsed by their efficiency, defined as the fraction of cell cycles in which they are used as in (McGuffee et al., 2013).

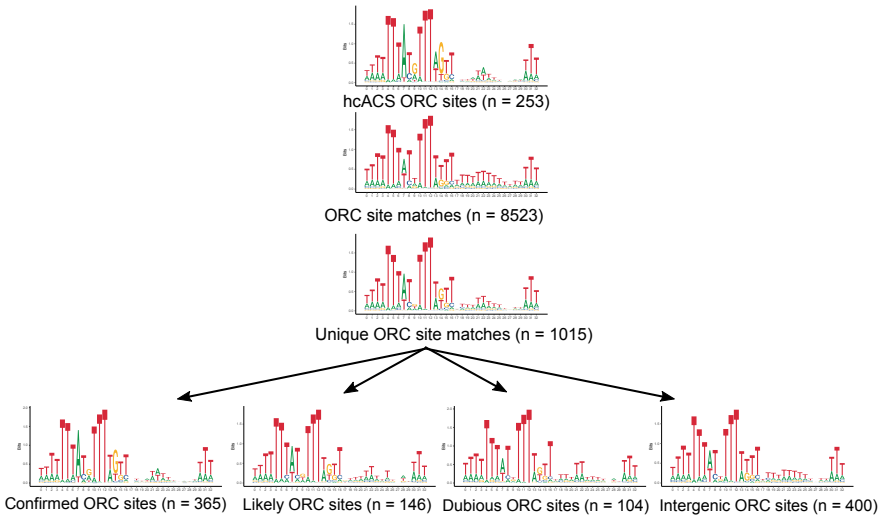

Figure S3: **Derivation of loci with unique matches to the ORC site to define the population of elements used for assessing Sir2-chromatin marks, MCM ChIP-seq, and Z-score assignments.**

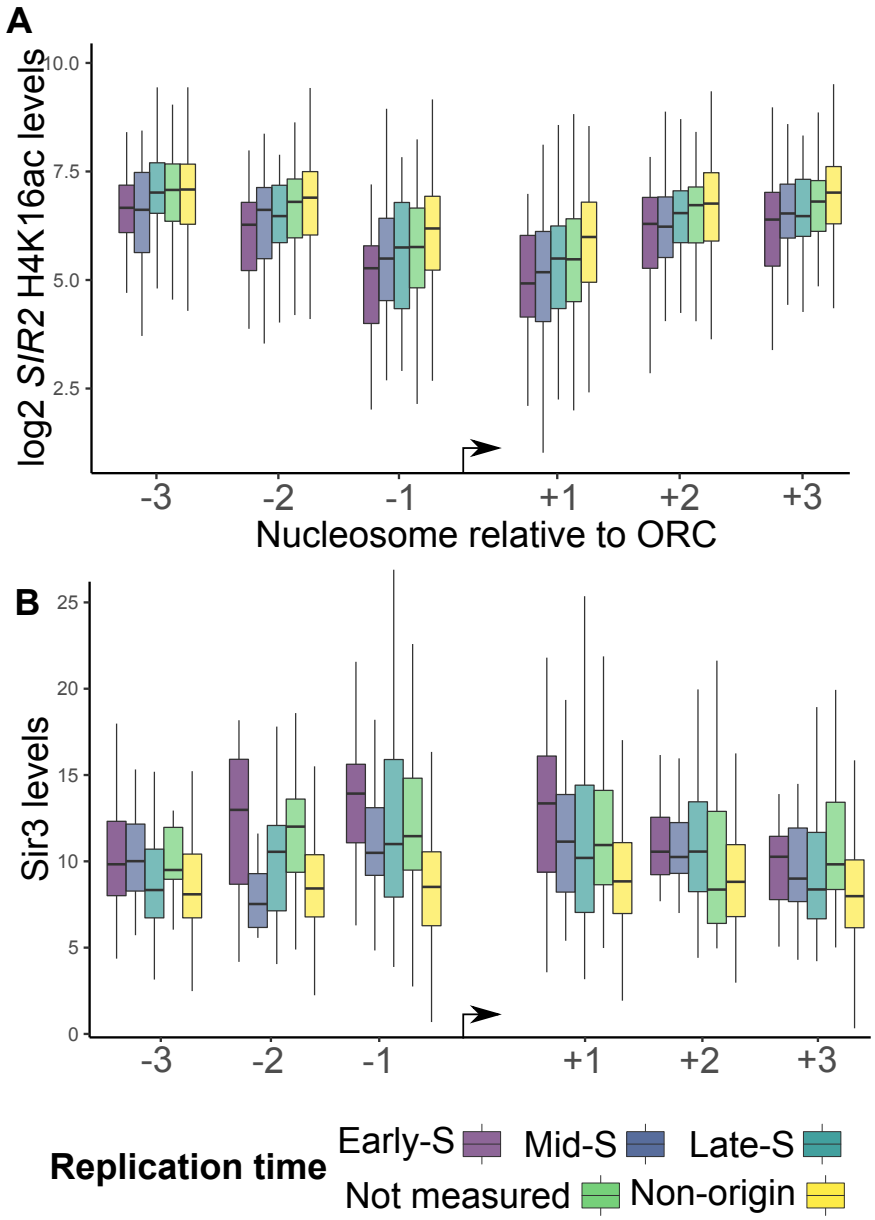

Figure S4: **Sir2-chromatin marks at the indicated loci.** **A.** Non-normalized H4K16ac levels on nucleosomes adjacent to the indicated euchromatic elements (Hoggard et al., 2018) **B.** Sir3 levels on same nucleosomes (Hoggard et al., 2018; Radman-Livaja et al., 2011). Note the inverse behavior of the two groups.

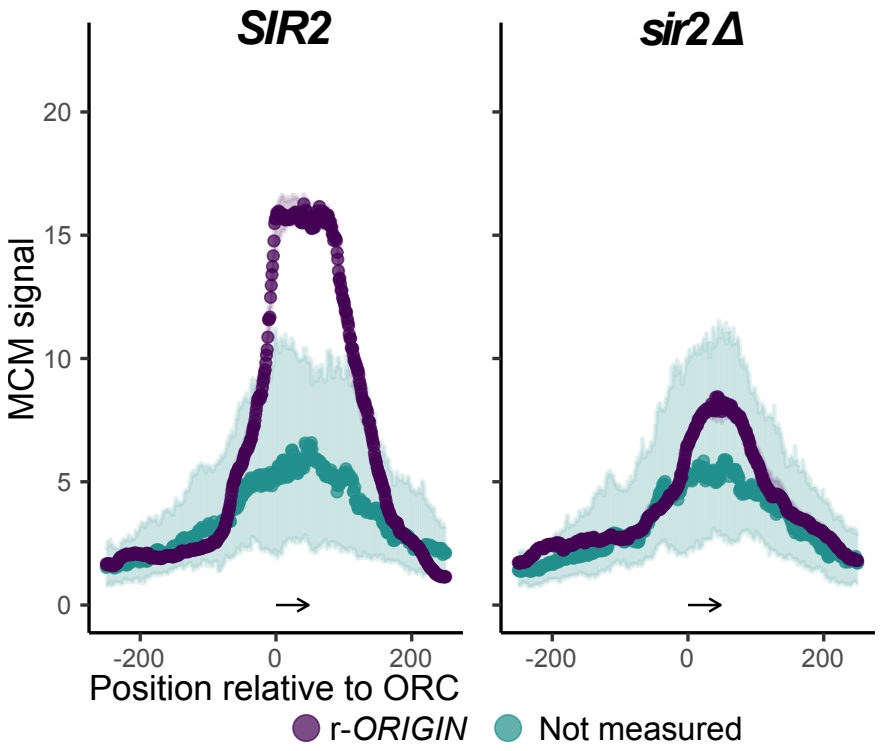

Figure S5: **Loss of *SIR2* did not enhance MCM association at the rDNA origin relative to the not-measured origin group.** Same approach as in Figure 4 only internally scaled rDNA origin (*r-ORIGIN*) locus is analyzed and shown in relation to the not-measured group of euchromatic origins.

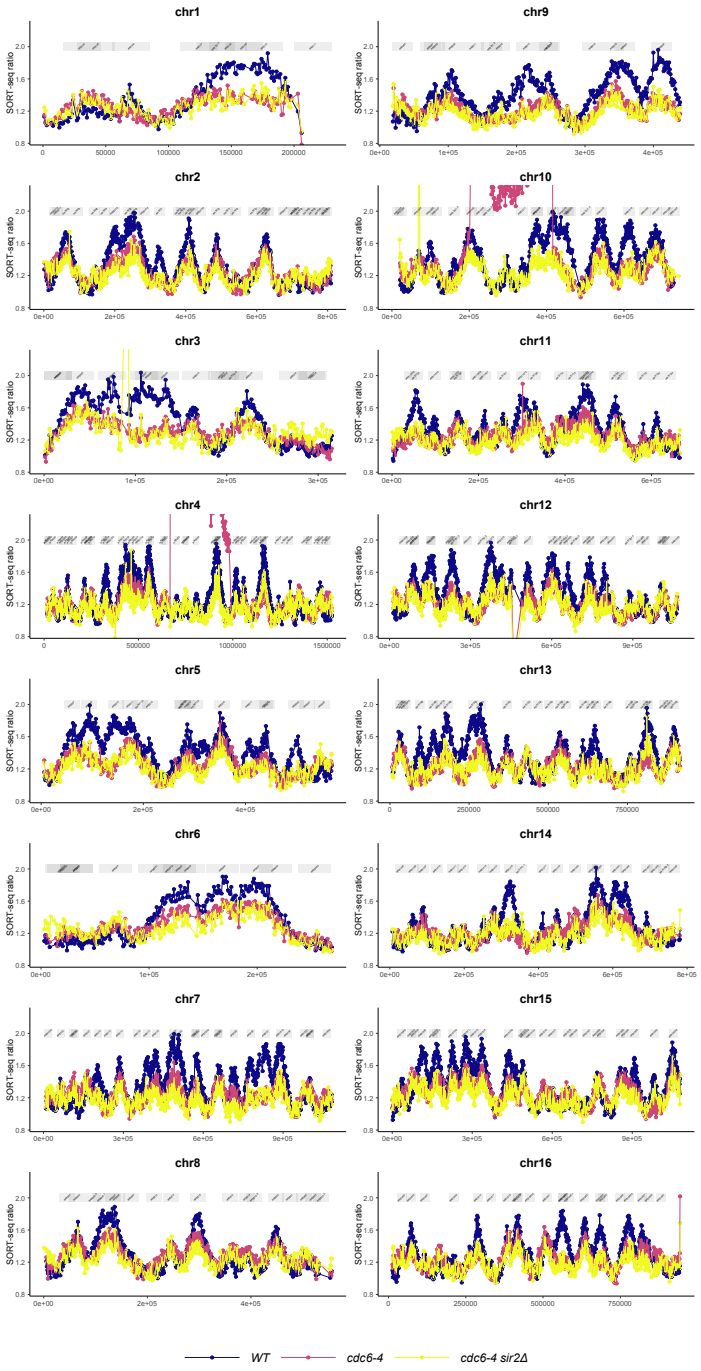

Figure S6: **Genome-wide Sort-Seq ratios.** The profiles show the relative normalized copy number ratio (y-axis) for each region on all chromosomes (x-axis). The dots represent the binned 1 kb ratios. Profiles are shown for wild-type (CFY4347, blue), *cdc6-4* (CFY4349, pink) and *cdc6-4 sir2Δ* (CFY4350, yellow) cells.

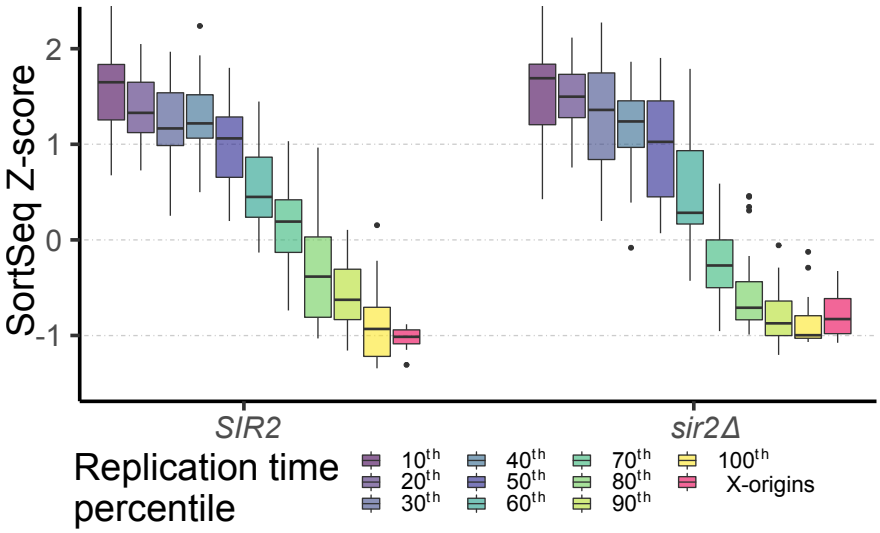

Figure S7: **Replication gap observed in an independent data set and in different strains.** Analyses of Sort-Seq data from (Foss et al., 2017) performed as in Figure 5D.

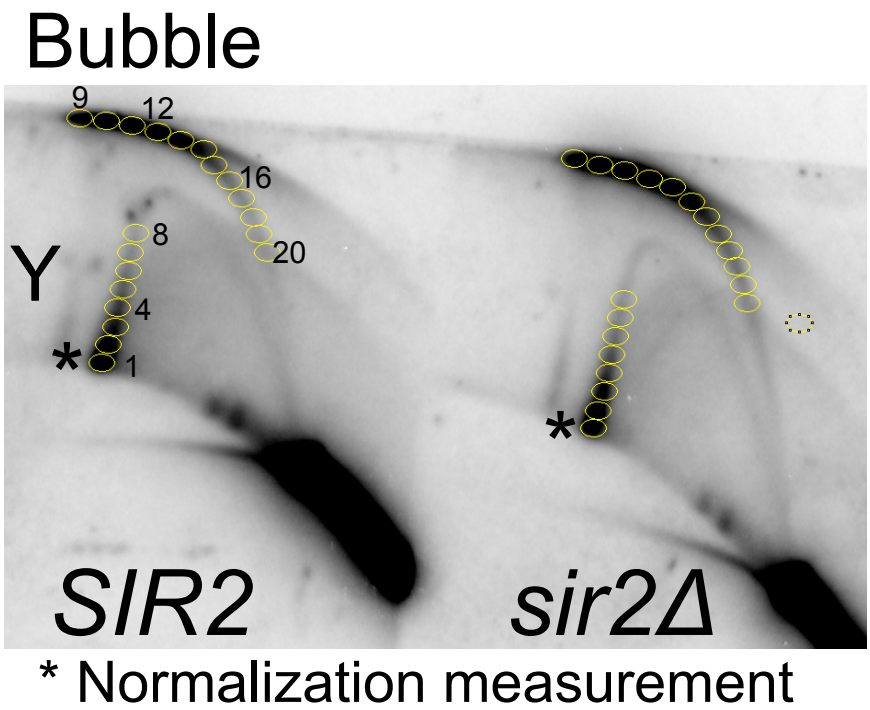

Figure S8: **Quantifying signals of replication-intermediates at ORI922 in *SIR2* and *sir2Δ?* cells.** The blot image file generated by the GE Typhoon Phosphorimager was imported into ImageJ 1.51q and processed by measuring the integrated intensities within the indicated circles of identical areas.

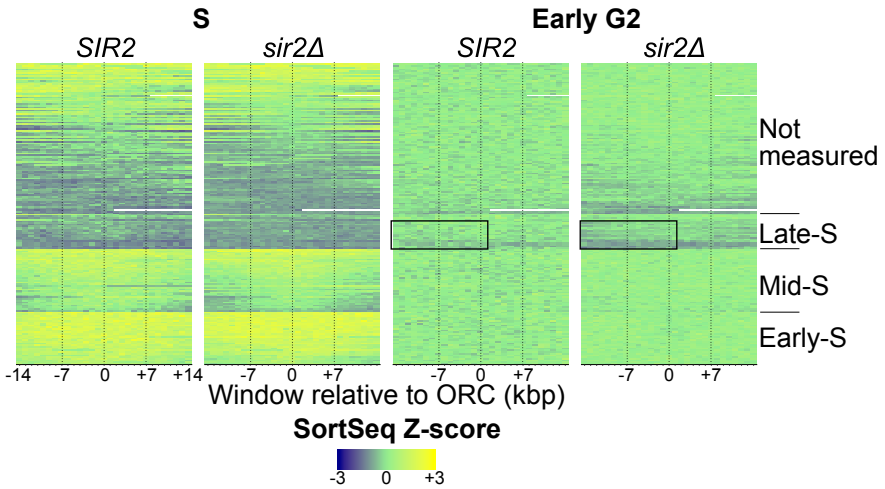

Figure S9: **Heat maps depicting Sort-Seq signals for indicated replicons.** Yeast replicons are on average ˜30 kb (Newman et al., 2013). To validate the Z-core analyses of the ORC site T-rich aligned 1 kb fragments in Figure 6, Z-scores were calculated for the summed ratios within fourteen unique 1 kb fragments 5' of the ORC site and fourteen unique fragments 3' of the ORC site. The 29 total windows spanned -14 through +14 kb (x-axis) for all assessed replicons. Each row on the y-axis contains the Z-scores spanning ˜28kb centered on the ORC site for each euchromatic origin analyzed in Figure 6. By including the additional 1 kb windows Z-scores, we can see that the behavior of the replicons are fully consistent with the Z-score assignments used in Figure 6. Boxed regions highlight the regions with low early G2 Z-scores in *sir2Δ* cells.

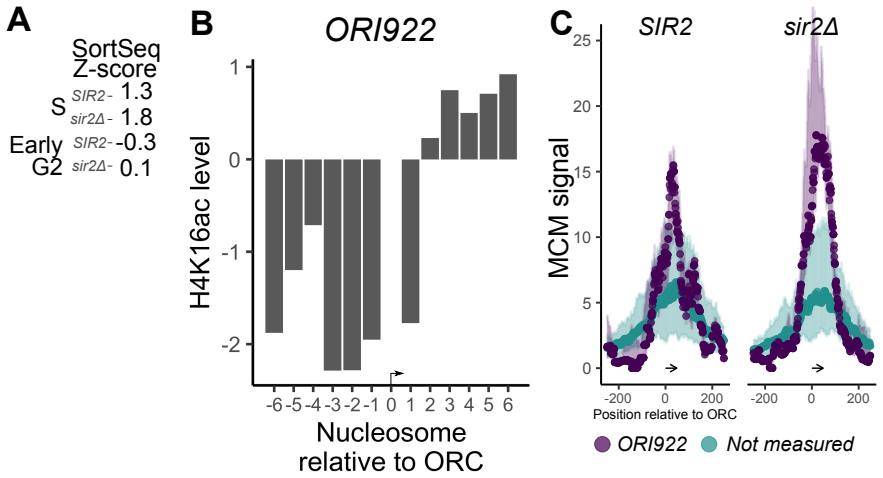

Figure S10: ***ORI922* data in this study: A.** Z-scores assigned to the *ORI922* fragment in indicated cells and cell-cycle phases from data presented in (Foss et al., 2017). **B.** Normalized H4K16ac levels in *SIR2* cells. **C.** Internally scaled MCM ChIP-Seq data.